Click here to access/download;Graphical Abstract (for review);DmPAC_graphicalAbstract.png

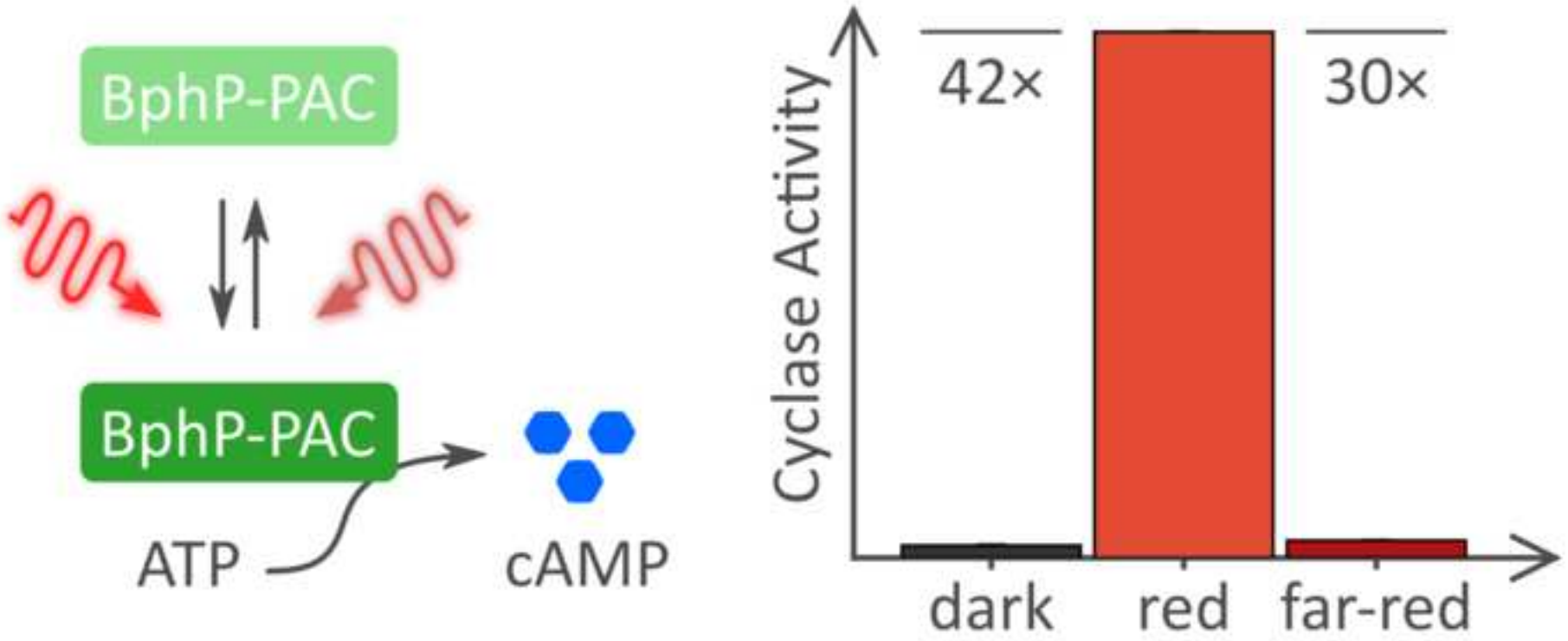

Highlights

- bacteriophytochromes (BphP) regulate effector function by red and far-red light
- recombining BphPs and cyclases generates photoactivated adenylyl cyclases (PAC)
- the variant *Dm*PAC exhibits 40-fold enhanced cyclase activity under red light
- the so-called PHY tongue governs PAC activity and light response
- *Dm*PAC affords optogenetic control of cyclic-nucleotide levels in mammalian cells

Marked Revision

Engineering bacteriophytochrome-coupled photoactivated adenylyl cyclases for enhanced optogenetic cAMP modulation

Qianzhao Xu[1], Arend Vogt[2], Fabian Frechen[3], Chengwei Yi[1], Melike Küçükerden[4-6], Neville Ngum[7], Laia Sitjà Roqueta[4-6], Andreas Greiner[8], Rhein Parri[7], Mercè Masana[4-6], Nikolaus Wenger[2], Dagmar Wachten[3], Andreas Möglich[1,9,10,*,‡]

[1] Department of Biochemistry, University of Bayreuth, 95447 Bayreuth, Germany.
[2] Charité – University Medicine Berlin, Department of Neurology with Experimental Neurology, 10117, Berlin, Germany.
[3] Institute of Innate Immunity, University of Bonn, 53127 Bonn, Germany.
[4] Department of Biomedical Sciences, Institute of Neuroscience, University of Barcelona, 08036 Barcelona, Spain.
[5] Institut d'Investigacions Biomèdiques August Pi i Sunyer (IDIBAPS), 08036 Barcelona, Spain.
[6] Centro de Investigación Biomédica en Red sobre Enfermedades Neurodegenerativas (CIBERNED), Spain.
[7] College of Health and Life Sciences, Aston University, Birmingham, B4 7ET, United Kingdom.
[8] Macromolecular Chemistry and Bavarian Polymer Institute, University of Bayreuth, Bayreuth 95440, Germany.
[9] Bayreuth Center for Biochemistry & Molecular Biology, Universität Bayreuth, 95447 Bayreuth, Germany.
[10] North-Bavarian NMR Center, Universität Bayreuth, 95447 Bayreuth, Germany.
* To whom correspondence should be addressed. Email: andreas.moeglich@uni-bayreuth.de
‡ ORCID identifiers: A.V. 0000-0003-0925-0308, F.F. 0009-0003-1279-2842, C.Y. 0000-0002-2167-4536, M.K. 0000-0002-4714-1666, L.S.R. 0000-0002-9584-5385, R.P. 0000-0002-1412-2688, M.M. 0000-0003-1392-4774, N.W. 0000-0002-0965-7530, D.W. 0000-0003-4800-6332, A.M. 0000-0002-7382-2772

Abstract

Sensory photoreceptors abound in nature and enable organisms to adapt behavior, development, and physiology to environmental light. In optogenetics, photoreceptors allow spatiotemporally precise, reversible, and non-invasive control by light of cellular processes. Notwithstanding the

development of numerous optogenetic circuits, an unmet demand exists for efficient circuits sensitive to red light, given its superior penetration of biological tissue. Bacteriophytochrome photoreceptors sense the ratio of red and far-red light to regulate the activity of enzymatic effector modules. The recombination of bacteriophytochrome photosensor modules with cyclase effectors underlies photoactivated adenylyl cyclases (PAC) that catalyze the synthesis of the ubiquitous second messenger 3', 5'-cyclic adenosine monophosphate (cAMP). Via homologous exchanges of the photosensor unit, we devised novel PACs, with the variant *Dm*PAC exhibiting 40-fold activation of cyclase activity under red light, thus surpassing previous red-light-responsive PACs. Modifications of the PHY tongue modulated the responses to red and far-red light. Exchanges of the cyclase effector offer an avenue to further enhancing PACs but require optimization of the linker to the photosensor. *Dm*PAC and a derivative for 3', 5'-cyclic guanosine monophosphate allow the manipulation of cyclic-nucleotide-dependent processes in mammalian cells by red light. Taken together, we advance the optogenetic control of second-messenger signaling and provide insight into the signaling and design of bacteriophytochrome receptors.

Keywords

cyclic nucleotide; optogenetics; phytochrome; second messenger; sensory photoreceptor; signal transduction; synthetic biology

Highlights

- bacteriophytochromes (BphP) regulate effector function by red and far-red light
- recombining BphPs and cyclases generates photoactivated adenylyl cyclases (PAC)
- the variant *Dm*PAC exhibits 40-fold enhanced cyclase activity under red light
- the so-called PHY tongue governs PAC activity and light response
- *Dm*PAC affords optogenetic control of cyclic-nucleotide levels in mammalian cells

Introduction

Sensory photoreceptor proteins enable organisms to sense light and, thereby, confer a sense of where and when. Physiological adaptations elicited by photoreceptors in response to photon absorption are generally reversible and precisely defined in space and time. Sensory photoreceptors group into several classes that are sensitive to different light bands within the near-UV to near-infrared (NIR) portion of the electromagnetic spectrum [1]. Originally identified in land plants [2] as ratiometric receptors of red (ca. 600-700 nm) and far-red, i.e., NIR, light (ca. 700-800 nm) [3], phytochromes (Phys) mediate vital processes, including photomorphogenesis and shade avoidance [4–6]. Informed by sequence homology, Phys were also discovered in bacteria where they control photoacclimation, photomorphogenesis, and virulence, among other processes [7–10]. Phys generally possess bipartite architecture with an N-terminal photosensory core module (PCM), comprising PAS (Per-ARNT-Sim [11]), GAF (cGMP-specific phosphodiesterases, adenylyl cyclases and FhlA [12]), and PHY domains [13–15], and a C-terminal output, or, effector, module (OPM), responsible for triggering downstream physiological responses. Sensitivity to red and NIR light is provided by bilin, i.e., linear tetrapyrrole, chromophores covalently attached to the PCM and nestling within its GAF entity. Conventional Phys adopt in darkness their red-light-absorbing Pr state with the bilin in the 15*Z* configuration of its C15=C16 double bond. Red light drives the conversion to the Pfr state that is sensitive to far-red light and is characterized by a 15*E*-configured bilin. The return to the dark-adapted Pr state either occurs passively in a slow thermal reaction or actively driven by far-red light. Bathyphytochromes differ from conventional Phys by assuming the Pfr form as their thermodynamically most stable state in darkness. Bilin *Z*/*E* isomerization couples to the OPM via a protrusion of the PHY domain, referred to as the PHY tongue, that undergoes a photoreversible transition between β-hairpin and α-helical conformations in the Pr and Pfr states, respectively [16–18]. The switch to the α-helical state engenders a compaction of the PHY tongue and, thereby, induces tertiary and quaternary structural changes that relay to the OPM [17,19].

Beyond natural photoreception, sensory photoreceptors also take center stage in optogenetics by serving as genetically encoded actuators for the control by light of cellular physiology, state, and processes [20–23]. Whereas plant Phys rely on light-dependent protein-protein interactions [5,24,25], bacterial Phys (BphP) achieve downstream responses by regulating the biological activity, mostly enzymatic, of covalently attached OPMs [22]. As exemplified by the thoroughly studied BphP from *Deinococcus radiodurans* (*Dr*BphP) [26], BphPs often harbor sensor histidine kinases as effectors that, together with cognate response regulators, form two-component

systems (TCS) [19,27]. Dependent on light, the sensor kinase catalyzes both the phosphorylation and dephosphorylation of the response regulator, and thus initiates downstream responses [19,28–30]. While light-sensitive TCSs are of immediate optogenetic utility [31–33] and support innovative use cases in bacterial biotechnology and synthetic biology [34], the *Dr*PCM can also be harnessed for regulating by red and far-red light disparate effector modules and physiological responses [22,35–37]. Such approaches are particularly pertinent for nucleotidyl cyclases [36,38,39] and phosphodiesterases (PDE) [35,40], arguably because these enzymes often occur naturally in conjunction with GAF regulatory modules [41]. By optogenetically regulating the making and breaking of cyclic mononucleotides, diverse processes reliant on these second messengers can be controlled across prokaryotes and eukaryotes [42]. Notably, BphP-coupled nucleotidyl cyclases and PDEs employ biliverdin as the chromophore which accrues in mammalian cells as a heme degradation product, thus allowing optogenetic deployment without exogenous chromophore addition as would be required for plant Phys [35,40,43]. Compared to other photoactivated adenylyl cyclases (PAC) that also produce 3', 5'-cyclic adenosine monophosphate (cAMP) [44–48], PACs based on BphP PCMs offer the advantage of sensitivity to red/NIR light which penetrates biological tissue more readily than visible light of shorter wavelengths [49]. However, the BphP-coupled PACs to date exhibit moderate dynamic ranges of photoactivation on the order of 10-fold or less [36,38,39] which pale in comparison to the up to several hundred-fold activity increase evidenced in the bacterial bPAC from *Beggiatoa* sp. under blue light [46,47]. For instance, the pioneering IlaC, engineered by connecting the *Rhodobacter sphaeroides* BphG1 PCM and the *Nostoc* sp. CyaB1 catalytic domain, exhibited a 6-fold acceleration of cAMP synthesis under red light compared to darkness [36]. Likewise, the recombination of the *Dr*PCM and the effector module of *Synechocystis* sp. PCC6803 Cya2 gave rise to PaaC which catalyzed cAMP formation around 4-fold more efficiently in red light than in darkness [38]. By replacing the *Dr*PCM in PaaC for the PCM from *Deinococcus deserti* BphP (*Dd*PCM), we generated *Dd*PAC with around 7-fold elevated adenylyl-cyclase activity under red light [39].

Against this backdrop, we here explored the modular construction of BphP-coupled adenylyl cyclases to obtain derivative and improved PACs. The variant *Dm*PAC, based on the PCM of the *Deinococcus maricopensis* BphP (*Dm*BphP), exhibited up to about 40-fold elevated cyclase activity under red light compared to far-red light or darkness, thus surpassing previous red-light-sensitive PACs. The PHY tongue proved key in governing the type and extent of the light response. Grafting the tongue of the *Dm*BphP onto other BphP-cyclases altered their responses to red and far-red light. Additional PAC variants can be obtained via exchange of the cyclase entity but require the

adjustment of the linker connecting the light-sensitive photosensor and catalytically active effector modules. Taken together, the present work informs the engineering of BphP-coupled enzymes. *Dm*PAC enables the optogenetic manipulation of cyclic-mononucleotide-dependent processes in the red and NIR spectral range.

Results

Modular Design of Photoactivated Adenylyl Cyclases

Earlier studies pinpointed PCM exchanges as a viable route towards altering and improving the traits of BphP-coupled enzymes [39,40,50,51]. As noted above, replacing the *Dr*PCM in PaaC [38] by the *Dd*PCM [39] yielded *Dd*PAC which exhibited a moderately higher dynamic range of light activation. Moreover, *Dd*PAC was not activated by NIR light around 850 nm which contrasts with the partial activation seen for PaaC [39]. Given these findings, we expanded our previous studies and assessed a much larger BphP PCM repertoire for their capability of regulating Cya2 and, prospectively, other nucleotidyl cyclases. A sequence alignment between PaaC, *Dd*PAC, and the PCMs from 19 additional BphPs guided the modular design of BphP-PACs (Suppl. Fig. S1). Notably, the Cya2 domain of these PACs bore the exchange of glutamate 488 to lysine which reprograms the cyclase product specificity from 3', 5'-cyclic guanosine monophosphate (cGMP) to cAMP [52].

To expedite functional screening and characterization, the PACs were constructed and tested in the pCyclR setup which comprises two plasmids [39] (Fig. 1a). The first plasmid drives the expression of a given BphP-PAC from a lactose-inducible T7-*lacO* promoter. An additional T7-*lacO* cassette included on the same plasmid encodes a heme oxygenase responsible for supplying the biliverdin chromophore. A second plasmid, denoted pCyclR, harbors a *Ds*Red Express2 red-fluorescent reporter under the control of the weak *lac* promoter. Both plasmids were transformed into the *Escherichia coli* CmpX13 Δ*cyaA* strain which features a knockout of the endogenous CyaA adenylyl cyclase [39]. Functional PAC expression ramps up the intracellular cAMP levels, thus activates the endogenous catabolite-activator protein (CAP), and in turn induces the expression of the *Ds*Red reporter from the *lac* promoter. The reporter fluorescence thereby provides an indirect readout of intracellular cAMP concentrations and cyclase activity.

CmpX13 Δ*cyaA* cells harboring the pCyclR plasmid and a pCDF expression vector encoding a given BphP-PAC were plated on solid medium containing 1 mM isopropyl-β-D-thiogalactopyranoside, followed by incubation at 37°C for 20 h in darkness, under red light [(660 ±

8) nm, 40 µW cm^{-2}], or under far-red light [(810 ± 15) nm, 240 µW cm^{-2}]. After incubation, the *Ds*Red fluorescence was measured and normalized by bacterial count. The readings were further normalized to that obtained for PaaC under red light which was assigned a value of 1 arbitrary unit (a.u.) (Fig. 1b). In darkness, the reporter fluorescence for PaaC was around 8.9-fold lower than under red light. As in our earlier characterization of PaaC, far-red light incurred a fluorescence increase by 5.2-fold relative to darkness. The initially surprising partial activation by far-red light can be rationalized by the emission spectrum of the NIR light-emitting diode (LED) used for illumination [53] (Fig. 1c). Although the emission peaked at 810 nm, its short-wavelength tail overlapped with the BphP Pr absorbance spectrum, thus principally accounting for the partial activation of PaaC. The previously characterized *Dd*PAC exhibited 8.4-fold higher reporter fluorescence under red light than in darkness. Far-red light also led to partial activation of *Dd*PAC with around 3-fold higher fluorescence than in darkness. By contrast, our earlier studies detected no *Dd*PAC activation by NIR light, albeit when using an 850-nm instead of an 810-nm LED [39]. We also tested the response of a PAC variant to several LEDs emitting in the NIR range (Suppl. Fig. S2). Most of these LEDs triggered a slight increase in pCyclR fluorescence, consistent with their emission spectra extending to shorter wavelengths around 700 to 730 nm.

The PAC variants based on the 19 other PCMs fell into three categories based on their reporter activity and light responses (Fig. 1b). First, several variants, e.g., *Is*PAC or *Ac*PAC based on the *Idiomarina* sp. and *Acaryochloris* sp. PCMs, respectively, displayed little reporter fluorescence regardless of illumination. Although the precise molecular origins remain unclear, the absence of reporter activity could principally owe to protein misfolding, insufficient chromophore incorporation, or disrupted catalytic activity. Given the lack of detectable light responses in the pCyclR setup, these variants were not pursued any further. Second, another category showed properties similar to PaaC and *Dd*PAC in that red light prompted increased reporter fluorescence and far-red light induced partial activation. Among the pertinent variants, *Dm*PAC, based on the PCM from *D. maricopensis*, showed the strongest fluorescence increase under red light of around 12.2-fold relative to darkness, while only exhibiting comparatively weak 1.8-fold activation by far-red light. Although the pCyclR platform merely provides indirect information on the molar adenylyl-cyclase activity and its dependence on light, we hypothesized that *Dm*PAC might prove superior to PaaC and *Dd*PAC. The third and largest category of PAC variants, exemplified by those based on the *P. aeruginosa* BphP (*Pa*BphP) and the *Agrobacterium fabrum* BphPs P1 (Agp1) and P2 (Agp2), were activated by red and far-red light to nearly the same extent. We note that several PCMs within this category were previously identified as bathyphytochromes with a Pfr dark-adapted state, for

185 instance *Pa*BphP [54] and Agp2 [55]. However, there is no strict correlation as Agp1 is a conventional
186 phytochrome that assumes the Pr state in darkness [56].

187

188 ## The PHY Tongue Governs the Light Responsiveness

189 We next assessed the different traits evident among certain PACs in more detail. Specifically, PaaC,
190 based on the *Dr*PCM, and *Dm*PAC exhibited markedly different responses to far-red light despite
191 47% sequence identity between their PCMs (Suppl. Fig. S1). Previous research on BphP PCMs
192 coupled to GGDEF effectors [51], i.e., diguanylate cyclases, revealed that the PHY tongue can govern
193 receptor activity and the extent of light regulation. The pivotal role of the PHY tongue is tied to its
194 conformational β→α transition upon Pr→Pfr photoconversion. As revealed by three-dimensional
195 structures of the *Dr*PCM [17,57] (Fig. 2a, b), the change from the Pr to the Pfr form entails a
196 shortening of the tongue that, in turn, promotes the swiveling apart of the PHY domains. We thus
197 reasoned that PHY tongue length may contribute to the light response in both natural and
198 engineered BphP receptors. A survey of around 13,900 proteins comprising PHY domains (Pfam [41]
199 family PF00360) revealed that the tongue varies in length by up to around ten residues (Fig. 2c),
200 with essentially all of the variation restricted to the leading part N-terminal of the conserved PRXSF
201 motif. Notably, the *Dr*PCM tongue is shorter by two to eight residues than those of the other 20
202 PCMs investigated at present (Fig. 2d). Across the PHY-containing proteins (Fig. 2c), this places the
203 *Dr*PCM within the bottom 3.9% of all tongue lengths.

204 To probe its role in light-dependent signal transduction, we replaced the PHY tongue in PaaC
205 by that from *Dm*PAC (Fig. 3a). Within the pCyclR setup, the resulting variant *Dm*Yt-PaaC resembled
206 PaaC in that red light (660 nm, 40 µW cm^{-2} intensity) elevated cyclase activity. However, in marked
207 contrast to PaaC, far-red light (810 nm, 240 µW cm^{-2}) hardly did. The converse introduction of the
208 PaaC tongue (originating from the *Dr*BphP) into *Dm*PAC had little effect on the responses to red and
209 far-red light (*Dr*Yt-*Dm*PAC). Guided by the PCM multiple sequence alignment, we next assessed
210 more limited tongue modifications in PaaC. Introduction of a DP dipeptide at the tongue N terminus
211 attenuated the response to far-red light as in *Dm*PAC (see Fig. 3a, PaaC-DP), whereas insertion of a
212 GTAR tetrapeptide directly before the PRXSF motif did not (PaaC-GTAR).

213 Prompted by these findings, we also grafted the *Dm* tongue onto Agp1PAC, Agp2PAC, *Hs*PAC,
214 *Js*PAC, *Pa*PAC, and *Sa*PAC (Fig. 3b-d, Suppl. Fig. S3), which are based on the BphPs from *A. fabrum*
215 P1 and P2, *Hymenobacter swuensis*, *Janthinobacter* sp., *P. aeruginosa*, and *Stigmatella aurantiaca*,

respectively (see Fig. 1b and Suppl. Fig. S1) [40]. In the following, we refer to the resulting tongue-substituted variants as *Dm*Yt-Agp1PAC, *Dm*Yt-Agp2PAC, *Dm*Yt-*Hs*PAC, *Dm*Yt-*Js*PAC, *Dm*Yt-*Pa*PAC, and *Dm*Yt-*Sa*PAC. When tested in the pCyclR assay, these variants showed light responses overall similar to those in the parental PACs (Fig. 3b-d, Suppl. Fig. S3). In certain PACs, e.g., *Dm*Yt-Agp1PAC, *Dm*Yt-*Js*PAC, and *Dm*Yt-*Sa*PAC, the tongue exchange lowered the basal cyclase activity in darkness. Under red light, the activity increased to similar values as in the parental PACs, except for *Dm*Yt-Agp2PAC where it was lower. Interestingly, the sensitivity of the tongue-exchanged variants to far-red light (810 nm) at 240 µW cm^{-2} intensity was essentially unaltered from that in the parental PACs, which contrasts with PaaC where the introduction of the *Dm* tongue entailed a reduced response to far-red light under these conditions. We hypothesized that the divergent properties might reflect different far-red light sensitivities in the tongue-exchanged PACs and next assessed their response to increased light intensities between 240 and 2,000 µW cm^{-2}. Indeed, elevated levels of far-red light successively reduced cyclase activity in five out of the six tongue-exchanged PACs (Agp1PAC, *Hs*PAC, *Js*PAC, *Pa*PAC, and *Sa*PAC). Solely, the variant derived from Agp2-PAC proved largely insensitive to increasing far-red light. To assess to which degrees these responses can be attributed to the PCMs or the replaced tongue, we next recorded the response of the parental PACs with their original PHY tongues to higher far-red-light levels (Fig. 3 and Suppl. Fig. S3) than used initially (see Fig. 1b). In marked contrast to the tongue-replaced variants, these PACs predominantly lacked clear-cut cyclase reduction at higher far-red-light doses. Solely, Agp2-PAC exhibited a pronounced activity decrease under intense far-red light. Apart from this exception, the *Dm* tongue thus rendered the light-induced Pfr→Pr reversion more efficient.

Analysis of Enhanced Photoactivated Adenylyl Cyclases

Based on the above data, we selected *Dm*PAC and *Pa*PAC for heterologous expression in *E. coli*, purification, and further analyses. UV-vis absorbance spectroscopy pinpointed *Dm*PAC as a conventional phytochrome that assumes its Pr state in darkness (Fig. 4a). Upon exposure to red light, *Dm*PAC converted to a 0.25:0.75 Pr:Pfr photostationary mixture (Suppl. Fig. S4), and illumination with far-red light prompted the complete reversion to the Pr state. When kept in darkness after exposure to red light, *Dm*PAC slowly recovered to its Pr state with a time constant of around (5,850 ± 60) s at 22°C (Fig. 4b). While the spectroscopic data are largely in line with the pCyclR results on *Dm*PAC (see Fig. 1b), it is worth noting that far-red light prompted a small increase in cyclase activity compared to darkness, whereas the absorbance spectra of *Dm*PAC in darkness and under far-red

light closely matched and revealed almost complete population of the Pr state. These findings can be rationalized by the partial absorption of the far-red LED emission by the Pr state of *Dm*PAC (see Fig. 1c). At photostationary state under prolonged far-red illumination, at any given time a small fraction of the *Dm*PAC molecules is converted to the Pfr state, thereby accounting for the slightly elevated adenylyl cyclase readout. Given the much better overlap between the far-red LED emission and the Pfr absorbance spectra, receptor molecules in the Pfr state are, however, rapidly returned to Pr, and the observable absorbance spectrum at photostationary state essentially corresponds to that of the pure Pr state.

By contrast, *Pa*PAC assumed its Pfr state in darkness, thus rendering it a bathyphytochrome like the parental *Pa*BphP (Fig. 4c). Illumination with 810-nm light led to a near-complete population of the Pr state, out of which *Pa*PAC thermally recovered to its Pfr dark-adapted state within around (287 ± 4) s (Fig. 4d). Exposure to red light gave rise to a 0.62:0.38 Pr:Pfr photostationary mixture (Suppl. Fig. S4), from which *Pa*PAC recovered to the Pfr state with essentially the same kinetics as from the Pr state. The correlation with the pCyclR data suggests that in *Pa*PAC the Pfr state is associated with the higher specific cyclase activity, whereas in *Dm*PAC the Pr state is more active. Moreover, the absorbance spectra of *Pa*PAC account for the observed activation of adenylyl cyclase activity by either red or far-red light, as observed in the pCyclR assay. The exposure to both red and far-red light drives the conversion of the Pfr to the Pr state, albeit to different extent. We also examined the *Dm*Yt-*Pa*PAC variant which differs from *Pa*PAC only in the sequence of its PHY tongue (Fig. 4e). Intriguingly, the tongue exchange sufficed for transforming this PAC into a conventional phytochrome with a Pr dark-adapted state. Red light drove conversion to a 0.51:0.49 Pr:Pfr mixture (Suppl. Fig. S4), and the subsequent dark recovery to the Pr state occurred with very slow kinetics over several hours (Fig. 4f). In addition to determining the nature of the dark-adapted state, the tongue evidently also governs the reversion kinetics to that state after photoactivation.

Next, we assessed the specific enzymatic activities of *Dm*PAC in darkness, red light, and far-red light. To this end, we incubated the PAC at different lighting conditions in the presence of excess substrate ATP. At certain time points, aliquots were drawn, rapidly arrested by heat denaturation, and analyzed by reversed-phase high-performance liquid chromatography (HPLC) (Fig. 5). The amounts of ATP and the reaction product cAMP were calculated based on absorbance measurements and comparison to standards. A linear fit to the reaction time course allowed the determination of specific enzymatic activities. Whereas in darkness the basal adenylyl cyclase activity was $(3.9 \pm 0.2) \times 10^{-3}$ nmol cAMP (mg *Dm*PAC × min)$^{-1}$, it increased by around 42-fold to (1.66

± 0.1) × 10^{-1} nmol cAMP (mg *Dm*PAC × min)$^{-1}$ in red light. Under far-red light, the activity amounted to (5.5 ± 0.1) × 10^{-3} nmol cAMP (mg *Dm*PAC × min)$^{-1}$ which is 1.4-fold higher than in darkness but 30-fold lower than in red light. To facilitate the comparison to previously reported PACs, we converted the specific enzymatic activities to molar activities, while implicitly assuming a fully active PAC preparation containing no inactive or misfolded protein. Doing so yielded apparent molar activities of (3.6 ± 0.2) × 10^{-4} mol cAMP (mol *Dm*PAC × min)$^{-1}$ in darkness, (1.5 ± 0.1) × 10^{-2} mol cAMP (mol *Dm*PAC × min)$^{-1}$ in red light, and (5.1 ± 0.1) × 10^{-4} mol cAMP (mol *Dm*PAC × min)$^{-1}$ under far-red light. By contrast, *Dd*PAC had shown apparent molar adenylyl cyclase activities of 8.8 × 10^{-3} mol cAMP (mol *Dd*PAC × min)$^{-1}$ and 6.1 × 10^{-2} mol cAMP (mol *Dd*PAC × min)$^{-1}$ in darkness and under red light, respectively, corresponding to a 7-fold difference [39]. Hence, *Dm*PAC exhibits a much better dynamic range of light regulation than *Dd*PAC, owing to its low basal activity in darkness. For comparison, the blue-light-responsive bPAC, the PAC most widely used in optogenetics, had apparent molar activities of 1.3 × 10^{-3} mol cAMP (mol bPAC × min)$^{-1}$ in darkness and 4.0 × 10^{-1} mol cAMP (mol bPAC × min)$^{-1}$ in blue light, i.e., a 300-fold difference, as probed by HPLC [47]. cPAC, a naturally occurring PAC with a cyanobacteriochrome photosensor unit, exhibited apparent molar activities of 0.29 mol cAMP (mol cPAC × min)$^{-1}$ in its dark-adapted P_b state and 0.86 mol cAMP (mol cPAC × min)$^{-1}$ in the P_g state populated upon blue-light absorption.

Control of Nucleotidyl Cyclase Activity in Mammalian Cells

To gauge the application scope in mammalian cells, we transfected *Dm*PAC into HEK-TM cells which stably express the cyclic-nucleotide gated (CNG) ion channel CNGA2-TM that opens upon binding cAMP and conducts cations [58]. To monitor adenylyl cyclase activity, the cells were loaded with the calcium-sensitive fluorophore FluoForte-AM. Intracellular cAMP production in the HEK-TM cells would hence prompt channel opening, influx of Ca^{2+} ions from the exterior, and elevated fluorescence. The PAC-transfected cells were incubated at 37°C in darkness, and FluoForte-AM fluorescence was monitored over time. The cells were exposed to red-light pulses (670 nm, 40 µW cm^{-2}) of different duration (1 or 10 s) at certain times, while continuously recording fluorescence (Fig. 6a). At the end of the experiment, the addition of ionomycin evoked a rapid Ca^{2+} influx and served to normalize the fluorescence signal. Cells transfected with *Dm*PAC reacted to red-light exposure with an increase in fluorescence, indicative of intracellular cAMP production and ion-channel opening. By contrast, non-transfected control cells showed no light responses. Notably, no biliverdin was added during these experiments, indicating that this chromophore was present in the

cells as a heme catabolism intermediate and that the PAC autonomously incorporated it. These data hence demonstrate that *Dm*PAC applies to the optogenetic control of cAMP levels and downstream processes in mammalian cells.

Signaling pathways dependent on cGMP are involved in many cellular processes but also in diseases [59–62]. To furnish an optogenetic tool for manipulating intracellular cGMP levels, we next restored the glutamate residue at position 488 in the Cya2 moiety of *Dm*PAC to revert the cyclase product specificity from cAMP to cGMP [52]. We examined the activity of the resultant photoactivated guanylyl cyclase, denoted *Dm*PGC, in HEK cells using the luminescence-based Glosensor assay, which banks on a genetically modified, cGMP-dependent firefly luciferase. HEK293 cells were co-transfected with *Dm*PGC and the cGMP biosensor (Fig. 6b). After overnight incubation of the transfected cells at 37°C in darkness, luciferin was added, and luminescence was monitored over time. When exposed to a 10-s red-light pulse (633 nm), the cells responded with a luminescence increase, indicative of photoactivated cGMP formation. The luminescence signal increased continuously until it reached a plateau after 10 min. Near-complete recovery to the baseline luminescence was observed within 90 minutes without additional illumination (measured at 29°C). By contrast, no effect was seen if the cells were kept in darkness nor when *Dm*PGC was combined with a cAMP-specific sensor.

Functional Exchange of the Cyclase Effector Necessitated Linker Adjustments

Having identified the *Dm*PCM as particularly adept at regulating nucleotidyl cyclase activity, we wondered whether it could also subject the activity of homologous cyclase effectors to control by red and far-red light. If so, this would pave the way towards the modular construction of yet additional PACs, potentially including specimens with enhanced activity and light responses. Informed by a multiple sequence alignment (Suppl. Fig. S5), we designed fusions between the *Dm*PCM and the effector domains of the adenylyl cyclases *Nostoc* sp. PCC 7120 CyaB1 and *Synechocystis* sp. PCC 6803 CyaA1. Notably, for the construction of the resultant receptors *Dm*(CyaB1) and *Dm*(CyaA1), we employed the same sequence register as in *Dm*PAC and PaaC [38]. That notwithstanding, the PAC variants initially showed low reporter activity and no or at most small light responses, when tested in the pCyclR assay. Merely, *Dm*(CyaA1) exhibited a twofold signal increase under red light compared to darkness.

Reasoning that the lack of clear-cut light responses could be due to poor thermodynamic coupling between the PCM and cyclase effector entities, we resorted to the PATCHY method [63] to systematically probe the length and sequence of the linker intervening the PCM and effector. Via suitable oligonucleotide primers and PCR amplification, we thus generated PATCHY libraries comprising PAC variants with linkers extended by up to twenty residues or shortened by up to twenty residues compared to the parental variant. The libraries were screened within the pCyclR assay under red light, and variants exhibiting elevated reporter fluorescence were selected for further analysis. In this manner, we identified a *Dm*(CyaB1) variant, denoted *Dm*CB1, with a linker shorter by four residues relative to the parental variant that showed a 16-fold activity increase under red light relative to darkness (Fig. 7). Similarly, certain *Dm*(CyaA1) variants with shortened linkers possessed red-light responses surpassing those of the parental constructs with the original linker composition. We further isolated a *Dm*(CyaB1) variant, termed *Dm*CB2, with a linker five residues longer than the parental variant and an inverted signal response, in that red light elicited a twofold reduction of activity compared to darkness, rather than an increase.

Discussion

Design of Bacteriophytochrome Enzymes

Leveraging the inherent modularity of bacteriophytochromes, we generated variants of red-light-regulated nucleotidyl cyclases by exchanging their constituent photosensor modules. The overall ready success of this design strategy (see Fig. 1b) suggests considerable mechanistic compatibility and hence interchangeability among BphP PCMs, as also observed previously [35,36,38–40,50,64,64]. Notably, the properties and degree of regulation varied across the light-responsive cyclase variants. Capitalizing on this variation, we identified *Dm*PAC which exhibits superior dynamic range of light regulation in enzymatic assays compared to previous BphP-coupled PACs (see Fig. 5). The modular exchange of photosensor modules therefore constitutes a viable engineering strategy towards derivatizing and potentially improving BphP-regulated enzymes and signal receptors in general.

The relative ease of creating derivative PACs with pronounced light responses starkly contrasts with the modular PCM exchange in BphP-regulated cyclic nucleotidyl phosphodiesterases (PDE) which proved demanding [40]. Any replacement of the *Dr*PCM, which underpins the original light-regulated PDE [35], abolished light responses [40], including for several of the same PCMs that supported robust light responses in the PACs at present. While the molecular reasons remain elusive,

the divergent findings in the PAC and PDE contexts may be rooted in initially inefficient coupling between the PCM photosensor and the PDE effector. Limited modifications at the PCM-effector junction installed light responses into otherwise light-inert PDEs [40]. In a similar vein, the modular exchange of the cyclase effector module presently resulted in absent or exceedingly poor light responses at first (see Fig. 7). Subsequent variations of the length and sequence of the linker conjoining the PCM and effector moieties led to enhanced cyclase activity and light responsiveness. The pronounced dependency on the linker properties can be explained by the structure of said linker which likely forms a continuous α helix and assembles into a coiled coil within the homodimeric receptor [19]. Similar linker variations were applied previously to the mechanistic characterization and optimization of bacteriophytochromes and other homodimeric sensory photoreceptors [29,35,36,38,63–65]. For instance, multiple IlaC variants were generated with linkers between their PCMs and adenylyl cyclase effectors extended in one-residue increments [36]. Several variants with linkers differing by ± 3 or 4 residues exhibited light-dependent adenylyl cyclase activity, consistent with a continuous α-helical structure of the linker and evidence in other engineered photoreceptors [29,35]. In a similar vein, the engineering of the derivative PACs IlaD and IlaM also involved the testing and optimization of α-helical linkers [66]. Closely related findings were obtained en route to the engineering of PagC (and its derivative PaaC) [38]. In particular, cyclase variants differing by 7 residues in their linker length exhibited alike light responses; by contrast, removal of a single residue from the linker sufficed for inverting the effect of light on cyclase activity. The crystal structure of PagC rationalized these findings in that it revealed a coiled-coil conformation of the linker within the homodimeric receptor, similar to findings for sensor histidine kinases [19,63,67,68]. A coiled-coil linker is also central to signal transduction in the BphP-GGDEF receptor *Is*PadC [64,65]. Red light is presumed to promote a transition between two registers within the coiled coil that give rise to differential activity of the GGDEF effector moiety. Appropriate linker length also proved decisive in the optogenetic control of receptor tyrosine kinases by the *Dr*PCM [37,69,70]. Modifications of the length and sequence of the linker intervening PCM and kinase strongly governed receptor activity and response to light. Finally, the crucial role of the linker connecting sensor and effector is further underlined by the marked preference for discrete linker lengths in several families of signal receptors in nature [11,71,72]. In summary, deliberate modifications of the photosensor-effector linker thus provide an efficient means of derivatizing and improving photoreceptor traits. As not least indicated by the present study, the systematic probing of linker traits unfolds its full potential if an efficient means of testing pertinent variants is at hand (see Fig. 1a, b).

Responses to Red and Far-red Light

Several of the light-responsive PAC variants generated and analyzed here not only reacted to red but also to far-red light around 810 nm (see Fig. 1c). Although this trait is to be expected for bathyphytochromes with a Pfr resting state, several of these PACs are based on PCMs described previously as conventional phytochromes with a Pr resting state. Moreover, we confirmed spectroscopically that *Dm*PAC assumes its Pr state both in darkness and when exposed to 810-nm light (see Fig. 4a). These observations seem in conflict to the pCyclR activity measurements which revealed activation, albeit weak, of cyclase activity in *Dm*PAC under far-red light. As noted above, the data can be reconciled by partial activation of the Pr→Pfr conversion by 810-nm light. This activation owes to the short-wavelength tail of the LED light source that partially overlaps with the Pr absorbance spectrum (see Fig. 1c). Although the reverse Pfr→Pr transition is driven much more readily by ~~far-red light~~the 810-nm LED than that from Pr to Pfr, at photostationary state a small fraction of the PAC molecules sample the Pfr state. This would account for the slight uptick in cyclase activity under 810-nm light. At the same time, the bulk of the molecules are in their Pr state as confirmed by absorbance spectroscopy. This model could potentially also account for the observed cyclase activity decrease at yet high higher 810-nm light levels (see Fig. 3). In this regime, both the Pr→Pfr and Pfr→Pr transitions could be sped up to the extent that the dwell time of the PAC in the Pfr state does not suffice for the elevated adenylyl cyclase activity to manifest.

Although it is unclear to what extent these aspects generally apply to BphP receptors, they might partially account for the sluggish and often incomplete activity reversion under far-red light after prior red-light exposure evidenced in several studies [35,39,40,73]. In an ideal scenario, the far-red light source employed for Pfr→Pr reversion should be configured to not trigger Pr→Pfr photoconversion at all. However, given the spectral overlap of the Pr and Pfr absorbance bands and the often-substantial width of the emission spectra of common light sources, this constellation may be hard to achieve. Therefore, and somewhat counterintuitively, partial activation of a BphP-based optogenetic circuit by far-red light cannot be ruled out upfront in optogenetic applications, and researchers should be mindful of such effects.

Importantly, our present data revealed differences among the BphP PCMs in their responses to light, specifically that in the far-red spectral range. These variations indicate a possible remedy for the inadvertent and usually undesired activation of BphP-based optogenetic implements by far-red light. Short of substituting the entire PCM (see Fig. 1b), more limited modifications to the receptor may suffice, for example within the PHY tongue (see Fig. 3). Commensurate with its

eminent role as a conduit between bilin isomerization and downstream conformational transitions [18], we pinpointed the PHY tongue as instrumental in governing light responses which concurs with insight on BphP-GGDEF receptors [51]. Introducing the PHY tongue of the *Dm*PCM (*Dm*Yt) into other PCMs led to enhanced downregulation of cyclase activity at elevated far-red light intensities. Put another way, the *Dm*Yt appeared to facilitate the light-driven return of the receptor to its low-activity Pr basal state. The pivotal role of the tongue is further underlined by the changes in photochemical properties evidenced in certain PACs upon introduction of the *Dm*Yt. Strikingly, the replacement of the PHY tongue of *Pa*PAC by the *Dm*Yt, corresponding to a change of less than a tenth of the residues in the receptor, reprogrammed this bathyphytochrome into a conventional Phy.

Photoactivated Nucleotidyl Cyclases as Optogenetic Implements

Through the construction and analyses of numerous PAC candidates containing different PCMs, we identified *Dm*PAC as an adenylyl cyclase with stringent regulation by red light. Given its pronounced regulatory response, *Dm*PAC may supersede *Dd*PAC [39] and other BphP-based adenylyl cyclases. We show *Dm*PAC to be suited for applications in mammalian cells to modulate cyclic mononucleotide levels and downstream responses. Importantly and consistent with earlier findings on BphP receptors [35,43], light responses could be evoked in the absence of biliverdin addition. In contrast to the more reduced bilin chromophores harnessed by plant Phys [22], biliverdin is apparently available in mammalian cells, exogenous chromophore addition is thus obviated, and full genetic encoding of BphP-based optogenetic tools is enabled [35,43]. The mutation of a single residue within the cyclase domain of *Dm*PAC yielded the guanylyl cyclase *Dm*PGC which produced cGMP rather than cAMP upon red-light exposure, thereby expanding the scope for applications in optogenetics. So far, we have deployed *Dm*PAC and *Dm*PGC only in cell culture but not in living animals. We caution that pertinent *in-vivo* applications may place additional demands on photoactivated nucleotidyl cyclases (and, in fact, other optogenetic tools as well), as aptly demonstrated by Gomelsky and colleagues [66]. Beyond stringent light responses, the optogenetic tool in question must also exhibit good expression and sufficient activity in animal hosts.

As the most widely used PAC, the blue-light-sensitive bPAC has higher molar activity than *Dm*PAC and an exquisite dynamic range of light regulation on the order of several hundred-fold, as determined by HPLC analyses [46,47]. bPAC has seen frequent use, for instance in the neurosciences to modulate synaptic plasticity [74,75]. Of more recent vintage, several cAMP-specific variants [76]

of the rhodopsin-based, photoactivated guanylyl cyclase RhoGC [77–79] were generated. When assessed in frog oocytes by enzyme-linked immunosorbent assays, these variants, denoted RhoAC, exhibited up to around hundred-fold higher maximal substrate turnover than bPAC (albeit, as measured by HPLC), low background activity, and stringent activation under green light by up to several hundred-fold and above [76]. Although *Dm*PAC falls short of this high efficiency, it is capable of evoking robust and relevant increases in nucleotidyl cyclase activity upon photostimulation. Of key advantage, *Dm*PAC possesses low basal activity and can be triggered by much longer wavelengths than either bPAC or RhoAC. The superior tissue penetration of longer wavelengths within the near-UV to NIR portion of the electromagnetic spectrum stands to bear for optogenetic applications in deep tissue, for example within the brain. In these scenarios, *Dm*PAC may be the tool of choice for optogenetically eliciting cyclic-mononucleotide-dependent physiological responses.

Materials and Methods

Molecular Biology

Bacteriophytochrome-regulated photoactivated adenylyl cyclases (BphP-PAC) were constructed in the pCDFDuet background (Novagen, Darmstadt, Germany) as previously for *Dd*PAC [39]. The pCDFDuet vector comprises two expression cassettes under the control of T7-*lacO* promoters, with one cassette encoding the BphP-PAC in question with a C-terminal hexahistidine tag, and the other one heme oxygenase 1 from *Synechocystis* sp. [40,80]. The BphP-PAC design was guided by a multiple sequence alignment between the PCMs of the BphPs, PagC [38], and *Dd*PAC [39] (Suppl. Fig. S1). The relevant PCMs derive from the BphPs of *D. radiodurans* (*Dr*, Uniprot identifier Q9RZA4), *D. deserti* (*Dd*, C1D3W9), *D. maricopensis* (*Dm*, E8U3T3), *Deinobacterium chartae* (*Dc*, A0A841HYA5), *Deinococcus peraridilitoris* (*Dp*, WP_157448871), *Deinococcus* sp. LM3 (*Dl*, OOV12932), *Acaryochloris* sp. CCMEE 5410 (*As*, WP_010479127), *A. fabrum* P1 (Agp1, Q7CY45), *A. fabrum* P2 (Agp2, A9CI81), *Agrobacterium vitis* (*Av*, B9JR96), *Azorhizobium caulinodans* (*Ac*, A8HU76), *Candidatus Gracilibacteria bacterium* (*Cg*, NJK50749), *Corallococcus coralloides* (*Cc*, H8MLG4), *Hymenobacter swuensis* (*Hs*, W8F0E4), *Idiomarina* sp. A28L (*Is*, F7RW09), *Janthinobacter* sp. CG23_2 (*Js*, CUI04487), *Pleurocapsa* sp. PCC 7319 (*Pl*, WP_019503487), *P. aeruginosa* (*Pa*, Q9HWR3), *Pseudomonas syringae* pv. *aptata* (*Ps*, KPZ04210), *Stigmatella aurantiaca* (*Sa*, Q097N3), and *Xanthomonas campestris* (*Xc*, A0A0H2XCS3). Likewise, cyclase sequences from *Nostoc* sp. PCC 7120 CyaB1 (Q7A2D9) and *Synechocystis* sp. PCC 6803 CyaA1 (P73823) were aligned to PagC which comprises the cyclase domain of *Synechocystis* sp. PCC6803 Cya2 (P72951) (Suppl. Fig. S5). All

sequence alignments were done with ClustalX2 [81]. The relevant PCM gene fragments were amplified by PCR with BphP-phosphodiesterases [40] or codon-optimized synthetic genes (GeneArt) as templates. The amplified PCR products were introduced into the pCDFDuet vector by Gibson cloning [82]. Tongue exchanges within the PCMs were generated by Gibson cloning or by PCR amplification and blunt-end ligation. Exchanges of the cyclase domains were performed by Gibson cloning using synthetic genes with *E. coli*-adapted codon usage as templates for PCR amplification. All primers are listed in Suppl. Tables S1-S3.

For the variation of linker length and sequence in BphP-PACs, the PATCHY strategy was applied [63]. To this end, template constructs were first generated in which the linkers between the BphP PCM and cyclase moieties were extended by 20 amino acids by PCR amplification with the primers listed in Suppl. Table S4 and subsequent blunt-end ligation. An additional DNA stretch between the linker segments deriving from the PCM and the cyclase, respectively, encoded a SmaI restriction site and a frameshift. For the incremental probing of the linker, forward primers were devised that annealed to the cyclase part of the linker and were iteratively staggered by three nucleotides (Suppl. Table S4). Likewise, staggered reverse primers annealing to the PCM linker were designed. The template constructs were then amplified by PCR with a mixture of all forward and reverse primers. The linear amplification products were purified, phosphorylated at their 5' termini by polynucleotide kinase, and ligated by T4 DNA ligase, followed by transformation into chemically competent *E. coli* XL1 Blue cells. The PATCHY libraries were screened for light-dependent cyclase activity within the pCyclR testbed described in the next section. The identity and sequence of all constructs were confirmed by DNA sequencing (Microsynth Seqlab, Göttingen).

PHY Tongue Analysis

A multiple sequence alignment (MSA) with 18,363 proteins comprising a PHY-specific domain (Pfam family PF00360 [41]) was downloaded from the InterPro database [83]. Using a custom Python script, the number of residues between and including two highly conserved residues bracketing the PHY tongue, residues W451 and W483 in *Dr*BphP, was counted. Entries in the MSA that had gaps at either or both the sequence positions aligned with W451 and W483 were disregarded. A histogram of the PHY tongue lengths in the remaining 13,901 entries within the MSA was plotted with Fit-o-mat [84].

Reporter-Gene Assays

The activity and light response of BphP-PAC variants were assessed with the pCyclR setup [39]. To this end, pCDFDuet plasmids encoding given variants were transformed into *E. coli* CmpX13 Δ*cyaA* cells harboring the pCyclR plasmid and a genomic knockout of the adenylyl cyclase CyaA. Transformed bacteria were plated on lysogeny broth (LB) agar supplemented with 50 µg mL^{-1} kanamycin, 100 µg mL^{-1} streptomycin, and 1 mM isopropyl-β-D-thiogalactopyranoside (IPTG), followed by incubation at 37°C for 20 h in darkness, under constant red light [(660 ± 8) nm, 40 µW cm^{-2}], or under constant far-red light [(810 ± 15) nm, 240-2,000 µW cm^{-2}]. All light intensities were determined with a model 842-PE power meter (Newport, Darmstadt, Germany) and a model 918D-UV-OD3 silicon photodetector (Newport). The emission spectra of the light-emitting diodes used in this study were determined with a SEC2022 diode-array spectrophotometer (ALS Instruments, Tokyo). After incubation, a portion of the cells were resuspended in 210 µL H_2O such that an optical density at 600 nm (OD_{600}) of around 0.4 was reached, as determined using a Tecan Infinite M200pro multimode microplate reader (Tecan, Männedorf, Switzerland). The cell suspension was then diluted 20-fold in H_2O, and fluorescence of the *Ds*Red Express2 [85] reporter gene was measured with the Tecan M200pro instrument at an excitation wavelength of (540 ± 9) nm and an emission wavelength of (591 ± 20) nm. Fluorescence values were normalized by OD_{600} and represent mean ± s.d. of at least three biologically independent replicates.

Protein Expression and Purification

pCDFDuet plasmids encoding BphP-PACs were transformed into chemically competent *E. coli* LOBSTR cells [86]. A single bacterial clone was used to inoculate a 5-mL LB starter culture supplemented with 100 µg mL^{-1} streptomycin (LB/Strep). After overnight incubation at 37°C, 1 mL of the culture was added to 800 mL LB/Strep in a baffled Erlenmeyer flask. The bacteria were cultured at 37°C and 225 rpm shaking until the OD_{600} reached around 1.0, at which point the temperature was lowered to 16°C, and 1 mM IPTG and 0.5 mM *δ*-aminolevulinic acid were added. Following 48 h incubation at 16°C and 100 rpm, bacteria were harvested by centrifugation and lysed by ultrasound. Purification was conducted similar to before [39]. Briefly, the cleared lysate was purified by Co^{2+} immobilized metal ion affinity chromatography. His-tagged BphP-PAC protein was eluted by an imidazole gradient from 0 to 1 M, and individual fractions were analyzed for protein content and purity by denaturing polyacrylamide gel electrophoresis. Fractions were pooled, dialyzed against storage buffer [20 mM Tris/HCl pH 8.0, 20 mM NaCl, 10% (v/v) glycerol], and

concentrated by spin filtration. Protein concentration was determined by UV/vis absorbance on an Agilent 8453 diode-array spectrophotometer (Agilent Technologies, Waldbronn, Germany) using a molar extinction coefficient of 86,200 M^{-1} cm^{-1} at 701 nm. Samples were flash-frozen in liquid nitrogen and stored at -80°C.

UV/vis Absorbance Spectroscopy

Absorbance measurements were done at 22°C on an Agilent 8453 spectrophotometer equipped with a Peltier thermostat. Spectra were recorded on dark-adapted samples and after saturating illumination with red light (630 nm) and far-red light (780 nm), respectively. Recovery kinetics were measured at 22°C. Samples were illuminated with saturating red or far-red light, respectively, and the return to the dark-adapted state was monitored at a wavelength of 780 nm. Instrumental drift was corrected by baseline measurements. The kinetics were fitted to exponential functions using Fit-o-mat [84].

The molar extinction coefficient of biliverdin within the *Dm*PCM was determined by comparing the UV/vis absorbance spectrum of the native holoprotein to that of the denatured holoprotein in 6 M guanidinium chloride [87,88]. These calculations were based on a molar extinction coefficient at 388 nm of 39,900 M^{-1} cm^{-1} for biliverdin in the denatured state, according to [88] and as done previously [35]. Inspection of the native spectrum yielded the molar extinction coefficient at 701 nm used above.

To correlate the Pr↔Pfr photoconversion with the reporter-gene data from the pCyclR assay, *Dm*PAC, *Pa*PAC, and *Dm*Yt-*Pa*PAC were also exposed to the same LEDs used in the pCyclR experiments. The resultant Pr:Pfr mixed-state spectra upon illumination with 660-nm or 810-nm light were evaluated according to Butler *et al.* [89].

High-Performance Liquid Chromatography

To assess the catalytic activity of *Dm*PAC, 10 µM of the enzyme was incubated at 30°C in 500 µL reaction buffer (50 mM HEPES/HCl pH 7.0, 150 mM NaCl, 50 mM $MgCl_2$). The reaction was started by adding 500 µM ATP. In parallel reactions, the reaction mixture was either kept in darkness, incubated under red light (633 nm, 80 µW cm^{-2}) [90], or exposed to far-red light (810 nm, 20 mW cm^{-2}). After 60, 120, 180, and 240 minutes, the reactions were arrested by heat inactivation at 95°C for 5 min. The resultant denatured protein was removed by centrifugation (16,100 × g, 10 min), and

the supernatant was filtered through a 0.2-µm filter (Macherey-Nagel, Düren, Germany). The amount of cAMP produced was analyzed by reversed-phase high-performance liquid chromatography (Agilent Technologies 1200 series). The samples were applied to a C18 column equilibrated with 20 mM ammonium acetate pH 3.7, 1% (v/v) acetonitrile. The isocratic elution was followed by absorbance at 253 nm. Substrate (ATP) and product (cAMP) were assigned and quantified by comparison to ATP and cAMP standards. Area integration of elution peaks was conducted with the Waters 2489 software. The production of cAMP was evaluated as a function of time where each timepoint corresponds to the mean ± s.d. of three independent replicates. The turnover of *Dm*PAC under the different illumination conditions was determined by fitting the reaction time courses to linear functions with Fit-o-mat. The experiment was repeated twice with similar outcome.

Cyclase Activity Assays in Mammalian Cells

Cyclase activity assays based on Ca^{2+} imaging in a fluorescence plate reader were performed as previously described [40,91,92]. To assess *Dm*PAC activity, HEK-TM cells stably expressing the CNGA2-TM ion channel were seeded on a PLL (0.1 mg mL^{-1}, Sigma Aldrich)-coated 96-well plate (F-Bottom, CELLSTAR, Greiner) at 2 x 10^4 cells per well and incubated over night at 37°C and 5% CO_2 in darkness. On the next day, the cells were transfected with Lipofectamine 3000 (Thermo Fisher Scientific) with pcDNA3.1-*Dm*PAC-FLAG3x. The transfection medium was replaced after 5-6 h with full medium. The cells were incubated overnight at 37°C and 5% CO_2 in darkness. All following steps were conducted under dim green light. The medium was removed, and cells were washed with 50 µL pre-warmed ES (extracellular solution) buffer (120 mM NaCl, 5 mM KCl, 2 mM $CaCl_2$, 2 mM $MgCl_2$, 10 mM glucose, 10 mM HEPES pH 7.4). Cells were loaded with 2 µM FluoForte-AM (Enzo Life Sciences, stocks in DMSO/Pluronic F-127 (Sigma-Aldrich)) and 3 mM probenecid (Invitrogen) in 50 µl ES for 30 min at 37°C. Afterwards, the buffer was replaced with 90 µL ES containing 3 mM probenecid, and cells were incubated for 30 min at 37°C in a fluorescence plate-reader (FLUOstar omega, BMG Labtech). Fluorescence was measured at 37°C with a 544-nm excitation and a (570 ± 10)-nm emission filter (filters BMG Labtech). For *Dm*PAC activity measurements, cells were supplemented with 25 µM of IBMX (250 mM stock in DMSO, AppliChem) five minutes before start of the measurements. During activity measurements, the cells were stimulated with a 670-nm-light pulse (40 µW cm^{-2}) for 1 s at 3 min and for 10 s at 21 min. At the end of the experiment, 2 µM ionomycin were added (1 mM stock in DMSO, Tocris), and fluorescence was recorded until

saturation of the signal amplitude. After the end of the recording, cell integrity and transfection rate were scrutinized by microscopy of the recorded wells.

For the experiments on *Dm*PGC, the original *Dm*PAC was cloned together with a C-terminal FLAG-tag into the pcDNA3.1 vector under control of the CMV promoter. Site-directed mutagenesis was used to introduce K488E mutation into the Cya2 domain [52] (see Suppl. Table S5 for primers). HEK293TN cells (System Biosciences, SBI) were cultured in DMEM+GlutaMAX medium (ThermoFisher Scientific) and seeded into white 96-well microplates (15,000 cells per well). After 24 h, the cells were transfected with plasmids for *Dm*PGC and the luciferase-based cGMP-biosensor plasmid pGloSensor-42F (Promega) according to the manufacturer's protocol but using XtremeGENE 9 (Roche Diagnostics) as transfection reagent. Again 24 h later, the medium in all wells was replaced with 80 µL per well of CO_2-independent Leibovitz's L-15 medium (ThermoFisher Scientific). Plates were incubated for at least another 12 h at 37°C in an incubator completely protected from light. DMEM- and L-15 medium were both supplemented with 10% fetal bovine serum and penicillin/streptomycin. For the final experiment, the cells were transferred into a Mithras LB 940 plate reader (Berthold Technologies). Luciferase substrate was added via injectors to each well (final volume of 90 µL per well with 0.6 mg mL^{-1} sodium D-Luciferin). The reader was set to 29°C, and luminescence was recorded with an integration time of 0.2 s per well. After 30 min of incubation, the plate was briefly removed from the reader and exposed to red-light LEDs (633 nm) for 15 s, while dark controls were covered. Luminescence was further measured for 90 min, and then sodium nitroprusside was added by injection as a light-independent positive control to a final concentration of 25 µM.

Acknowledgements

Financial support was provided by the European Commission (FET Open NEUROPA, grant 863214 to M.M., R.P., and A.M.), the Deutsche Forschungsgemeinschaft (grant MO2192/4-2 to A.M., SFB 1454 project 432325352 to D.W., TRR333/1 project 450149205 to D.W., EXC2151 project 390873048 to D.W.), the Else Kröner Fresenius Foundation (2021.EKFSE.53 to D.W.), the Young Investigator Project OptoImmun (DFG SPP1926 to A.V.), intramural funding from the University of Bonn (to D.W.), a Freigeist fellowship by the Volkswagen Stiftung (to N.W.), the Spanish Ministry of Sciences, Innovation and Universities (PID2021-124896OA-I00 and María de Maeztu Unit of Excellence, Institute of Neurosciences, University of Barcelona, CEX2021-001159-M to M.M.). This work is

dedicated to Prof. Silvia E. Braslavsky, a pioneer in photobiology and photobiophysics, on her 80th birthday.

References

[1] A. Möglich, X. Yang, R.A. Ayers, K. Moffat, Structure and function of plant photoreceptors, Annu. Rev. Plant Biol. 61 (2010) 21–47. doi:10.1146/annurev-arplant-042809-112259.

[2] W.L. Butler, K.H. Norris, H.W. Siegelman, S.B. Hendricks, Detection, Assay, and Preliminary Purification of the Pigment Controlling Photoresponsive Development of Plants, Proc. Natl. Acad. Sci. 45 (1959) 1703–1708.

[3] N.C. Rockwell, J.C. Lagarias, A brief history of phytochromes, Chemphyschem. 11 (2010) 1172–1180. doi:10.1002/cphc.200900894.

[4] G. Bae, G. Choi, Decoding of Light Signals by Plant Phytochromes and Their Interacting Proteins, Annu. Rev. Plant Biol. 59 (2008) 281–311. doi:10.1146/annurev.arplant.59.032607.092859.

[5] V.N. Pham, P.K. Kathare, E. Huq, Phytochromes and Phytochrome Interacting Factors, Plant Physiol. 176 (2018) 1025–1038. doi:10.1104/pp.17.01384.

[6] N.C. Rockwell, J.C. Lagarias, Phytochrome evolution in 3D: deletion, duplication, and diversification, New Phytol. 225 (2020) 2283–2300. doi:10.1111/nph.16240.

[7] J. Hughes, T. Lamparter, F. Mittmann, E. Hartmann, W. Gärtner, A. Wilde, T. Börner, A prokaryotic phytochrome, Nature. 386 (1997) 663. doi:10.1038/386663a0.

[8] S.J. Davis, A.V. Vener, R.D. Vierstra, Bacteriophytochromes: Phytochrome-Like Photoreceptors from Nonphotosynthetic Eubacteria, Science. 286 (1999) 2517–2520. doi:10.1126/science.286.5449.2517.

[9] N.C. Woitowich, A.S. Halavaty, P. Waltz, C. Kupitz, J. Valera, G. Tracy, K.D. Gallagher, E. Claesson, T. Nakane, S. Pandey, G. Nelson, R. Tanaka, E. Nango, E. Mizohata, S. Owada, K. Tono, Y. Joti, A.C. Nugent, H. Patel, A. Mapara, J. Hopkins, P. Duong, D. Bizhga, S.E. Kovaleva, R. St. Peter, C.N. Hernandez, W.B. Ozarowski, S. Roy-Chowdhuri, J.-H. Yang, P. Edlund, H. Takala, J. Ihalainen, J. Brayshaw, T. Norwood, I. Poudyal, P. Fromme, J.C.H. Spence, K. Moffat, S. Westenhoff, M. Schmidt, E.A. Stojkovic, Structural basis for light control of cell development revealed by crystal structures of a myxobacterial phytochrome, IUCrJ. 5 (2018) 619–634. doi:10.1107/S2052252518010631.

[10] F. Gan, G. Shen, D.A. Bryant, Occurrence of Far-Red Light Photoacclimation (FaRLiP) in Diverse Cyanobacteria, Life. 5 (2015) 4–24. doi:10.3390/life5010004.

[11] A. Möglich, R.A. Ayers, K. Moffat, Structure and signaling mechanism of Per-ARNT-Sim domains, Structure. 17 (2009) 1282–1294. doi:10.1016/j.str.2009.08.011.

[12] L. Aravind, C.P. Ponting, The GAF domain: an evolutionary link between diverse phototransducing proteins, Trends Biochem Sci. 22 (1997) 458–9.

[13] L.O. Essen, J. Mailliet, J. Hughes, The structure of a complete phytochrome sensory module in the Pr ground state, Proc Natl Acad Sci U A. 105 (2008) 14709–14714.

[14] X. Yang, J. Kuk, K. Moffat, Crystal structure of Pseudomonas aeruginosa bacteriophytochrome: Photoconversion and signal transduction, Proc Natl Acad Sci U A. 105 (2008) 14715–14720.

[15] H. Li, E.S. Burgie, Z.T.K. Gannam, H. Li, R.D. Vierstra, Plant phytochrome B is an asymmetric dimer with unique signalling potential, Nature. 604 (2022) 127–133. doi:10.1038/s41586-022-04529-z.

[16] K. Anders, G. Daminelli-Widany, M.A. Mroginski, D. von Stetten, L.-O. Essen, Structure of the cyanobacterial phytochrome 2 photosensor implies a tryptophan switch for phytochrome signaling, J. Biol. Chem. 288 (2013) 35714–35725. doi:10.1074/jbc.M113.510461.
[17] H. Takala, A. Björling, O. Berntsson, H. Lehtivuori, S. Niebling, M. Hoernke, I. Kosheleva, R. Henning, A. Menzel, J.A. Ihalainen, S. Westenhoff, Signal amplification and transduction in phytochrome photosensors, Nature. 509 (2014) 245–248. doi:10.1038/nature13310.
[18] H. Takala, P. Edlund, J.A. Ihalainen, S. Westenhoff, Tips and turns of bacteriophytochrome photoactivation, Photochem. Photobiol. Sci. 19 (2020) 1488–1510. doi:10.1039/D0PP00117A.
[19] A. Möglich, Signal transduction in photoreceptor histidine kinases, Protein Sci. 28 (2019) 1923–1946. doi:10.1002/pro.3705.
[20] K. Deisseroth, G. Feng, A.K. Majewska, G. Miesenböck, A. Ting, M.J. Schnitzer, Next-generation optical technologies for illuminating genetically targeted brain circuits, J. Neurosci. 26 (2006) 10380–10386. doi:10.1523/JNEUROSCI.3863-06.2006.
[21] A. Losi, K.H. Gardner, A. Möglich, Blue-Light Receptors for Optogenetics, Chem. Rev. 118 (2018) 10659–10709. doi:10.1021/acs.chemrev.8b00163.
[22] K. Tang, H.M. Beyer, M.D. Zurbriggen, W. Gärtner, The Red Edge: Bilin-Binding Photoreceptors as Optogenetic Tools and Fluorescence Reporters, Chem. Rev. 121 (2021) 14906–14956. doi:10.1021/acs.chemrev.1c00194.
[23] E.S. Boyden, F. Zhang, E. Bamberg, G. Nagel, K. Deisseroth, Millisecond-timescale, genetically targeted optical control of neural activity, Nat. Neurosci. 8 (2005) 1263–1268. doi:10.1038/nn1525.
[24] D. Golonka, P. Fischbach, S.G. Jena, J.R.W. Kleeberg, L.-O. Essen, J.E. Toettcher, M.D. Zurbriggen, A. Möglich, Deconstructing and repurposing the light-regulated interplay between Arabidopsis phytochromes and interacting factors, Commun. Biol. 2 (2019) 448. doi:10.1038/s42003-019-0687-9.
[25] D. Golonka, U. Gerken, J. Köhler, A. Möglich, The Association Kinetics Encode the Light Dependence of Arabidopsis Phytochrome B Interactions, J. Mol. Biol. 432 (2020) 4327–4340. doi:10.1016/j.jmb.2020.06.001.
[26] S.-H. Bhoo, S.J. Davis, J. Walker, B. Karniol, R.D. Vierstra, Bacteriophytochromes are photochromic histidine kinases using a biliverdin chromophore, Nature. 414 (2001) 776–779. doi:10.1038/414776a.
[27] A. Buschiazzo, F. Trajtenberg, Two-Component Sensing and Regulation: How Do Histidine Kinases Talk with Response Regulators at the Molecular Level?, Annu. Rev. Microbiol. 73 (2019) null. doi:10.1146/annurev-micro-091018-054627.
[28] F.D. Russo, T.J. Silhavy, The essential tension: opposed reactions in bacterial two-component regulatory systems, Trends Microbiol. 1 (1993) 306–310.
[29] A. Möglich, R.A. Ayers, K. Moffat, Design and signaling mechanism of light-regulated histidine kinases, J. Mol. Biol. 385 (2009) 1433–1444. doi:10.1016/j.jmb.2008.12.017.
[30] E. Multamäki, R. Nanekar, D. Morozov, T. Lievonen, D. Golonka, W.Y. Wahlgren, B. Stucki-Buchli, J. Rossi, V.P. Hytönen, S. Westenhoff, J.A. Ihalainen, A. Möglich, H. Takala, Comparative analysis of two paradigm bacteriophytochromes reveals opposite functionalities in two-component signaling, Nat. Commun. 12 (2021) 4394. doi:10.1038/s41467-021-24676-7.
[31] R. Ohlendorf, R.R. Vidavski, A. Eldar, K. Moffat, A. Möglich, From dusk till dawn: one-plasmid systems for light-regulated gene expression, J. Mol. Biol. 416 (2012) 534–542. doi:10.1016/j.jmb.2012.01.001.
[32] J.J. Tabor, A. Levskaya, C.A. Voigt, Multichromatic control of gene expression in Escherichia coli, J. Mol. Biol. 405 (2011) 315–324. doi:10.1016/j.jmb.2010.10.038.

[33] E. Multamäki, A. García de Fuentes, O. Sieryi, A. Bykov, U. Gerken, A.T. Ranzani, J. Köhler, I. Meglinski, A. Möglich, H. Takala, Optogenetic Control of Bacterial Expression by Red Light, ACS Synth. Biol. 11 (2022) 3354–3367. doi:10.1021/acssynbio.2c00259.
[34] R. Ohlendorf, A. Möglich, Light-regulated gene expression in Bacteria: Fundamentals, advances, and perspectives, Front. Bioeng. Biotechnol. 10 (2022). https://www.frontiersin.org/articles/10.3389/fbioe.2022.1029403.
[35] C. Gasser, S. Taiber, C.-M. Yeh, C.H. Wittig, P. Hegemann, S. Ryu, F. Wunder, A. Möglich, Engineering of a red-light-activated human cAMP/cGMP-specific phosphodiesterase, Proc. Natl. Acad. Sci. U. S. A. 111 (2014) 8803–8808. doi:10.1073/pnas.1321600111.
[36] M.-H. Ryu, I.-H. Kang, M.D. Nelson, T.M. Jensen, A.I. Lyuksyutova, J. Siltberg-Liberles, D.M. Raizen, M. Gomelsky, Engineering adenylate cyclases regulated by near-infrared window light, Proc. Natl. Acad. Sci. U. S. A. 111 (2014) 10167–10172. doi:10.1073/pnas.1324301111.
[37] A.V. Leopold, K.G. Chernov, A.A. Shemetov, V.V. Verkhusha, Neurotrophin receptor tyrosine kinases regulated with near-infrared light, Nat. Commun. 10 (2019) 1–13. doi:10.1038/s41467-019-08988-3.
[38] S. Etzl, R. Lindner, M.D. Nelson, A. Winkler, Structure-guided design and functional characterization of an artificial red light–regulated guanylate/adenylate cyclase for optogenetic applications, J. Biol. Chem. 293 (2018) 9078–9089. doi:10.1074/jbc.RA118.003069.
[39] B. Stüven, R. Stabel, R. Ohlendorf, J. Beck, R. Schubert, A. Möglich, Characterization and engineering of photoactivated adenylyl cyclases, Biol. Chem. 400 (2019) 429–441. doi:10.1515/hsz-2018-0375.
[40] R. Stabel, B. Stüven, J.N. Hansen, H.G. Körschen, D. Wachten, A. Möglich, Revisiting and Redesigning Light-Activated Cyclic-Mononucleotide Phosphodiesterases, J. Mol. Biol. 431 (2019) 3029–3045. doi:10.1016/j.jmb.2019.07.011.
[41] R.D. Finn, J. Mistry, B. Schuster-Böckler, S. Griffiths-Jones, V. Hollich, T. Lassmann, S. Moxon, M. Marshall, A. Khanna, R. Durbin, S.R. Eddy, E.L. Sonnhammer, A. Bateman, Pfam: clans, web tools and services, Nucleic Acids Res. 34 (2006) D247–D251.
[42] V. Jansen, J.F. Jikeli, D. Wachten, How to control cyclic nucleotide signaling by light, Curr. Opin. Biotechnol. 48 (2017) 15–20. doi:10.1016/j.copbio.2017.02.014.
[43] K.D. Piatkevich, F.V. Subach, V.V. Verkhusha, Far-red light photoactivatable near-infrared fluorescent proteins engineered from a bacterial phytochrome, Nat. Commun. 4 (2013) 2153. doi:10.1038/ncomms3153.
[44] M. Iseki, S. Matsunaga, A. Murakami, K. Ohno, K. Shiga, K. Yoshida, M. Sugai, T. Takahashi, T. Hori, M. Watanabe, A blue-light-activated adenylyl cyclase mediates photoavoidance in *Euglena gracilis*, Nature. 415 (2002) 1047–1051. doi:10.1038/4151047a.
[45] S. Schröder-Lang, M. Schwärzel, R. Seifert, T. Strünker, S. Kateriya, J. Looser, M. Watanabe, U.B. Kaupp, P. Hegemann, G. Nagel, Fast manipulation of cellular cAMP level by light in vivo, Nat. Methods. 4 (2007) 39–42. doi:10.1038/nmeth975.
[46] M.-H. Ryu, O.V. Moskvin, J. Siltberg-Liberles, M. Gomelsky, Natural and engineered photoactivated nucleotidyl cyclases for optogenetic applications, J. Biol. Chem. 285 (2010) 41501–41508. doi:10.1074/jbc.M110.177600.
[47] M. Stierl, P. Stumpf, D. Udwari, R. Gueta, R. Hagedorn, A. Losi, W. Gärtner, L. Petereit, M. Efetova, M. Schwarzel, T.G. Oertner, G. Nagel, P. Hegemann, Light-modulation of cellular cAMP by a small bacterial photoactivated adenylyl cyclase, bPAC, of the soil bacterium beggiatoa, J. Biol. Chem. 286 (2011) 1181–1188. doi:10.1074/jbc.M110.185496.
[48] S. Raffelberg, L. Wang, S. Gao, A. Losi, W. Gärtner, G. Nagel, A LOV-domain-mediated blue-light-activated adenylate (adenylyl) cyclase from the cyanobacterium Microcoleus chthonoplastes PCC 7420, Biochem. J. 455 (2013) 359–365. doi:10.1042/BJ20130637.

[49] R. Weissleder, A clearer vision for *in vivo* imaging, Nat. Biotechnol. 19 (2001) 316–317. doi:10.1038/86684.
[50] M.-H. Ryu, M. Gomelsky, Near-infrared light responsive synthetic c-di-GMP module for optogenetic applications, ACS Synth. Biol. 3 (2014) 802–810. doi:10.1021/sb400182x.
[51] G. Gourinchas, U. Vide, A. Winkler, Influence of the N-terminal segment and the PHY-tongue element on light-regulation in bacteriophytochromes, J. Biol. Chem. (2019) jbc.RA118.007260. doi:10.1074/jbc.RA118.007260.
[52] A. Rauch, M. Leipelt, M. Russwurm, C. Steegborn, Crystal structure of the guanylyl cyclase Cya2, Proc. Natl. Acad. Sci. 105 (2008) 15720–15725. doi:10.1073/pnas.0808473105.
[53] S.G. Sokolovski, E.A. Zherebtsov, R.K. Kar, D. Golonka, R. Stabel, N.B. Chichkov, A. Gorodetsky, I. Schapiro, A. Möglich, E.U. Rafailov, Two-photon conversion of a bacterial phytochrome, Biophys. J. 120 (2021) 964–974. doi:10.1016/j.bpj.2021.01.028.
[54] R. Tasler, T. Moises, N. Frankenberg-Dinkel, Biochemical and spectroscopic characterization of the bacterial phytochrome of Pseudomonas aeruginosa, FEBS J. 272 (2005) 1927–1936. doi:10.1111/j.1742-4658.2005.04623.x.
[55] B. Karniol, R.D. Vierstra, The pair of bacteriophytochromes from Agrobacterium tumefaciens are histidine kinases with opposing photobiological properties, Proc. Natl. Acad. Sci. 100 (2003) 2807–2812. doi:10.1073/pnas.0437914100.
[56] T. Lamparter, N. Michael, F. Mittmann, B. Esteban, Phytochrome from Agrobacterium tumefaciens has unusual spectral properties and reveals an N-terminal chromophore attachment site, Proc. Natl. Acad. Sci. 99 (2002) 11628–11633. doi:10.1073/pnas.152263999.
[57] E.S. Burgie, J. Zhang, R.D. Vierstra, Crystal Structure of Deinococcus Phytochrome in the Photoactivated State Reveals a Cascade of Structural Rearrangements during Photoconversion, Structure. 24 (2016) 448–457. doi:10.1016/j.str.2016.01.001.
[58] S. Wachten, J. Schlenstedt, R. Gauss, A. Baumann, Molecular identification and functional characterization of an adenylyl cyclase from the honeybee, J. Neurochem. 96 (2006) 1580–1590. doi:10.1111/j.1471-4159.2006.03666.x.
[59] M.P. Kelly, Cyclic nucleotide signaling changes associated with normal aging and age-related diseases of the brain, Cell. Signal. 42 (2018) 281–291. doi:10.1016/j.cellsig.2017.11.004.
[60] R. Feil, M. Lehners, D. Stehle, S. Feil, Visualising and understanding cGMP signals in the cardiovascular system, Br. J. Pharmacol. 179 (2022) 2394–2412. doi:10.1111/bph.15500.
[61] A. Jehle, O. Garaschuk, The Interplay between cGMP and Calcium Signaling in Alzheimer's Disease, Int. J. Mol. Sci. 23 (2022) 7048. doi:10.3390/ijms23137048.
[62] E.K. Argyrousi, P.R.A. Heckman, J. Prickaerts, Role of cyclic nucleotides and their downstream signaling cascades in memory function: Being at the right time at the right spot, Neurosci. Biobehav. Rev. 113 (2020) 12–38. doi:10.1016/j.neubiorev.2020.02.004.
[63] R. Ohlendorf, C.H. Schumacher, F. Richter, A. Möglich, Library-Aided Probing of Linker Determinants in Hybrid Photoreceptors, ACS Synth. Biol. 5 (2016) 1117–1126. doi:10.1021/acssynbio.6b00028.
[64] G. Gourinchas, S. Etzl, C. Göbl, U. Vide, T. Madl, A. Winkler, Long-range allosteric signaling in red light-regulated diguanylyl cyclases, Sci. Adv. 3 (2017) e1602498. doi:10.1126/sciadv.1602498.
[65] G. Gourinchas, U. Heintz, A. Winkler, Asymmetric activation mechanism of a homodimeric red light-regulated photoreceptor, ELife. 7 (2018) e34815. doi:10.7554/eLife.34815.
[66] A. Fomicheva, C. Zhou, Q.-Q. Sun, M. Gomelsky, Engineering Adenylate Cyclase Activated by Near-Infrared Window Light for Mammalian Optogenetic Applications, ACS Synth. Biol. 8 (2019) 1314–1324. doi:10.1021/acssynbio.8b00528.

[67] R.P. Diensthuber, M. Bommer, T. Gleichmann, A. Möglich, Full-length structure of a sensor histidine kinase pinpoints coaxial coiled coils as signal transducers and modulators, Structure. 21 (2013) 1127–1136. doi:10.1016/j.str.2013.04.024.
[68] W.Y. Wahlgren, E. Claesson, I. Tuure, S. Trillo-Muyo, S. Bódizs, J.A. Ihalainen, H. Takala, S. Westenhoff, Structural mechanism of signal transduction in a phytochrome histidine kinase, Nat. Commun. 13 (2022) 7673. doi:10.1038/s41467-022-34893-3.
[69] A.V. Leopold, S. Thankachan, C. Yang, D. Gerashchenko, V.V. Verkhusha, A general approach for engineering RTKs optically controlled with far-red light, Nat. Methods. 19 (2022) 871–880. doi:10.1038/s41592-022-01517-z.
[70] A.V. Leopold, S. Pletnev, V.V. Verkhusha, Bacterial Phytochrome as a Scaffold for Engineering of Receptor Tyrosine Kinases Controlled with Near-Infrared Light, J. Mol. Biol. 432 (2020) 3749–3760. doi:10.1016/j.jmb.2020.04.005.
[71] N.C. Rockwell, R. Ohlendorf, A. Möglich, Cyanobacteriochromes in full color and three dimensions, Proc. Natl. Acad. Sci. U. S. A. 110 (2013) 806–807. doi:10.1073/pnas.1220690110.
[72] S.T. Glantz, E.J. Carpenter, M. Melkonian, K.H. Gardner, E.S. Boyden, G.K.-S. Wong, B.Y. Chow, Functional and topological diversity of LOV domain photoreceptors, Proc. Natl. Acad. Sci. U. S. A. 113 (2016) E1442-1451. doi:10.1073/pnas.1509428113.
[73] A.A. Kaberniuk, M. Baloban, M.V. Monakhov, D.M. Shcherbakova, V.V. Verkhusha, Single-component near-infrared optogenetic systems for gene transcription regulation, Nat. Commun. 12 (2021) 3859. doi:10.1038/s41467-021-24212-7.
[74] S. Yang, O.M. Constantin, D. Sachidanandan, H. Hofmann, T.C. Kunz, V. Kozjak-Pavlovic, T.G. Oertner, G. Nagel, R.J. Kittel, C.E. Gee, S. Gao, PACmn for improved optogenetic control of intracellular cAMP, BMC Biol. 19 (2021) 227. doi:10.1186/s12915-021-01151-9.
[75] Z. Zhou, K. Okamoto, J. Onodera, T. Hiragi, M. Andoh, M. Ikawa, K.F. Tanaka, Y. Ikegaya, R. Koyama, Astrocytic cAMP modulates memory via synaptic plasticity, Proc. Natl. Acad. Sci. 118 (2021) e2016584118. doi:10.1073/pnas.2016584118.
[76] U. Scheib, M. Broser, O.M. Constantin, S. Yang, S. Gao, S. Mukherjee, K. Stehfest, G. Nagel, C.E. Gee, P. Hegemann, Rhodopsin-cyclases for photocontrol of cGMP/cAMP and 2.3 Å structure of the adenylyl cyclase domain, Nat. Commun. 9 (2018) 2046. doi:10.1038/s41467-018-04428-w.
[77] G.M. Avelar, R.I. Schumacher, P.A. Zaini, G. Leonard, T.A. Richards, S.L. Gomes, A Rhodopsin-Guanylyl Cyclase Gene Fusion Functions in Visual Perception in a Fungus, Curr. Biol. 24 (2014) 1234–1240. doi:10.1016/j.cub.2014.04.009.
[78] U. Scheib, K. Stehfest, C.E. Gee, H.G. Körschen, R. Fudim, T.G. Oertner, P. Hegemann, The rhodopsin–guanylyl cyclase of the aquatic fungus Blastocladiella emersonii enables fast optical control of cGMP signaling, Sci Signal. 8 (2015) rs8–rs8. doi:10.1126/scisignal.aab0611.
[79] S. Gao, J. Nagpal, M.W. Schneider, V. Kozjak-Pavlovic, G. Nagel, A. Gottschalk, Optogenetic manipulation of cGMP in cells and animals by the tightly light-regulated guanylyl-cyclase opsin CyclOp, Nat. Commun. 6 (2015) 8046. doi:10.1038/ncomms9046.
[80] K. Mukougawa, H. Kanamoto, T. Kobayashi, A. Yokota, T. Kohchi, Metabolic engineering to produce phytochromes with phytochromobilin, phycocyanobilin, or phycoerythrobilin chromophore in Escherichia coli, FEBS Lett. 580 (2006) 1333–1338. doi:10.1016/j.febslet.2006.01.051.
[81] M.A. Larkin, G. Blackshields, N.P. Brown, R. Chenna, P.A. McGettigan, H. McWilliam, F. Valentin, I.M. Wallace, A. Wilm, R. Lopez, J.D. Thompson, T.J. Gibson, D.G. Higgins, Clustal W and Clustal X version 2.0, Bioinformatics. 23 (2007) 2947–2948. doi:10.1093/bioinformatics/btm404.

[82] D.G. Gibson, L. Young, R.-Y. Chuang, J.C. Venter, C.A. Hutchison, H.O. Smith, Enzymatic assembly of DNA molecules up to several hundred kilobases, Nat. Methods. 6 (2009) 343–345. doi:10.1038/nmeth.1318.
[83] M. Blum, H.-Y. Chang, S. Chuguransky, T. Grego, S. Kandasaamy, A. Mitchell, G. Nuka, T. Paysan-Lafosse, M. Qureshi, S. Raj, L. Richardson, G.A. Salazar, L. Williams, P. Bork, A. Bridge, J. Gough, D.H. Haft, I. Letunic, A. Marchler-Bauer, H. Mi, D.A. Natale, M. Necci, C.A. Orengo, A.P. Pandurangan, C. Rivoire, C.J.A. Sigrist, I. Sillitoe, N. Thanki, P.D. Thomas, S.C.E. Tosatto, C.H. Wu, A. Bateman, R.D. Finn, The InterPro protein families and domains database: 20 years on, Nucleic Acids Res. 49 (2021) D344–D354. doi:10.1093/nar/gkaa977.
[84] A. Möglich, An Open-Source, Cross-Platform Resource for Nonlinear Least-Squares Curve Fitting, J. Chem. Educ. 95 (2018) 2273–2278. doi:10.1021/acs.jchemed.8b00649.
[85] R.L. Strack, D.E. Strongin, D. Bhattacharyya, W. Tao, A. Berman, H.E. Broxmeyer, R.J. Keenan, B.S. Glick, A noncytotoxic DsRed variant for whole-cell labeling, Nat. Methods. 5 (2008) 955–957. doi:10.1038/nmeth.1264.
[86] K.R. Andersen, N.C. Leksa, T.U. Schwartz, Optimized E. coli expression strain LOBSTR eliminates common contaminants from His-tag purification, Proteins Struct. Funct. Bioinforma. 81 (2013) 1857–1861. doi:10.1002/prot.24364.
[87] M. Storf, A. Parbel, M. Meyer, B. Strohmann, H. Scheer, M.-G. Deng, M. Zheng, M. Zhou, K.-H. Zhao, Chromophore Attachment to Biliproteins: Specificity of PecE/PecF, a Lyase-Isomerase for the Photoactive 31-Cys-α84-phycoviolobilin Chromophore of Phycoerythrocyanin, Biochemistry. 40 (2001) 12444–12456. doi:10.1021/bi010776s.
[88] X. Shu, A. Royant, M.Z. Lin, T.A. Aguilera, V. Lev-Ram, P.A. Steinbach, R.Y. Tsien, Mammalian expression of infrared fluorescent proteins engineered from a bacterial phytochrome, Science. 324 (2009) 804–807. doi:10.1126/science.1168683.
[89] W.L. Butler, S.B. Hendricks, H.W. Siegelman, ACTTON SPECTRA OF PHYTOCHROME IN VITRO, Photochem. Photobiol. 3 (1964) 521–528. doi:10.1111/j.1751-1097.1964.tb08171.x.
[90] J. Hennemann, R.S. Iwasaki, T.N. Grund, R.P. Diensthuber, F. Richter, A. Möglich, Optogenetic Control by Pulsed Illumination, Chembiochem. 19 (2018) 1296–1304. doi:10.1002/cbic.201800030.
[91] V. Jansen, L. Alvarez, M. Balbach, T. Strünker, P. Hegemann, U.B. Kaupp, D. Wachten, Controlling fertilization and cAMP signaling in sperm by optogenetics, ELife. 4 (2015). doi:10.7554/eLife.05161.
[92] J.N. Hansen, F. Kaiser, C. Klausen, B. Stüven, R. Chong, W. Bönigk, D.U. Mick, A. Möglich, N. Jurisch-Yaksi, F.I. Schmidt, D. Wachten, Nanobody-directed targeting of optogenetic tools to study signaling in the primary cilium, ELife. 9 (2020) e57907. doi:10.7554/eLife.57907.
[93] E.S. Burgie, T. Wang, A.N. Bussell, J.M. Walker, H. Li, R.D. Vierstra, Crystallographic and Electron Microscopic Analyses of a Bacterial Phytochrome Reveal Local and Global Rearrangements during Photoconversion*, J. Biol. Chem. 289 (2014) 24573–24587. doi:10.1074/jbc.M114.571661.

Figures

Figure 1

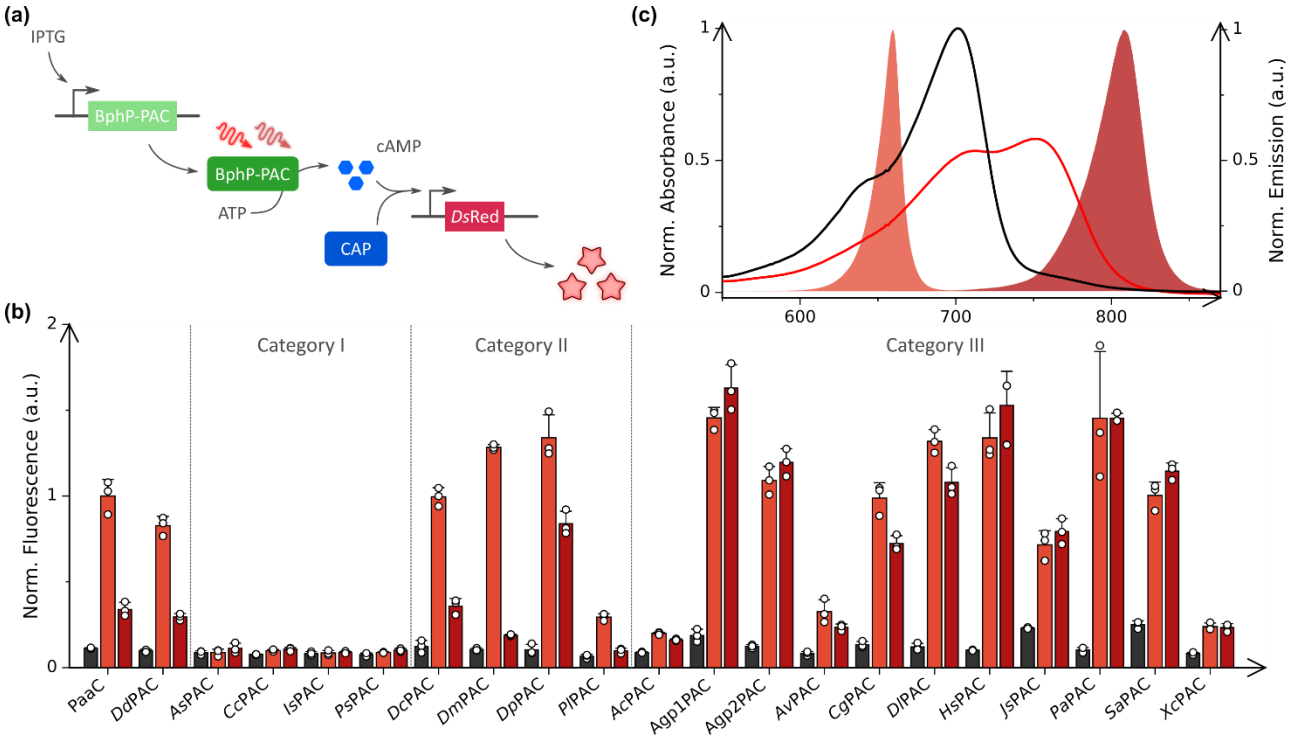

Engineering and characterization of photoactivated adenylyl cyclases (PAC). **(a)** Schematic of the pCyclR reporter-gene assay [39]. *E. coli ΔcyaA* cells are transformed with a plasmid encoding heme oxygenase and the PAC of interest. Once induced by IPTG and functionally expressed *in situ*, the PAC mediates the intracellular production of 3', 5'-cyclic adenosine monophosphate (cAMP). In turn, cAMP binds to the catabolite activator protein (CAP), thereby allowing it to activate the expression of the red-fluorescent reporter *Ds*Red. **(b)** pCyclR reporter results for PAC variants comprising one of 21 different BphP PCMs coupled to the cyclase effector module from *Synechocystis sp.* PCC 6803 Cya2. Species abbreviations are *A. caulinodans* (*Ac*), *Acaryochloris* sp. CCMEE 5410 (*As*), *A. fabrum* P1 (Agp1), *A. fabrum* P2 (Agp2), *A. vitis* (*Av*), *Candidatus Gracilibacteria bacterium* (*Cg*), *C. coralloides* (*Cc*), *D. radiodurans* (*Dr*), *D. deserti* (*Dd*), *D. maricopensis* (*Dm*), *D. chartae* (*Dc*), *D. peraridilitoris* (*Dp*), *Deinococcus* sp. LM3 (*Dl*), *H. swuensis* (*Hs*), *Idiomarina* sp. A28L (*Is*), *Janthinobacter* sp. CG23_2 (*Js*), *Pleurocapsa* sp. PCC 7319 (*Pl*), *P. aeruginosa* (*Pa*), *P. syringae* (*Ps*), *S. aurantiaca* (*Sa*), and *X. campestris* (*Xc*). Note that PaaC is based on the PCM from *D. radiodurans* [38]. Bacterial cultures were grown in darkness (black bars), under constant red light (red bars, 40 µW cm^{-2}, 660 nm), or under constant far-red light (brown bars, 240 µW cm^{-2}, 810 nm). Based on their activity and light responses, the PAC variants were assigned to one of three categories (see main text). *Ds*Red fluorescence readings were normalized by the optical density of the

bacterial cultures at 600 nm. Data represent mean ± s.d. of three biologically independent samples, shown as white dots. **(c)** Absorbance spectra of the *Dm*PCM in its dark-adapted state (black) and after exposure to red light (red). The filled curves show the emission spectra of the red and far-red LEDs used throughout the study for driving Pr↔Pfr photoconversion.

Figure 2

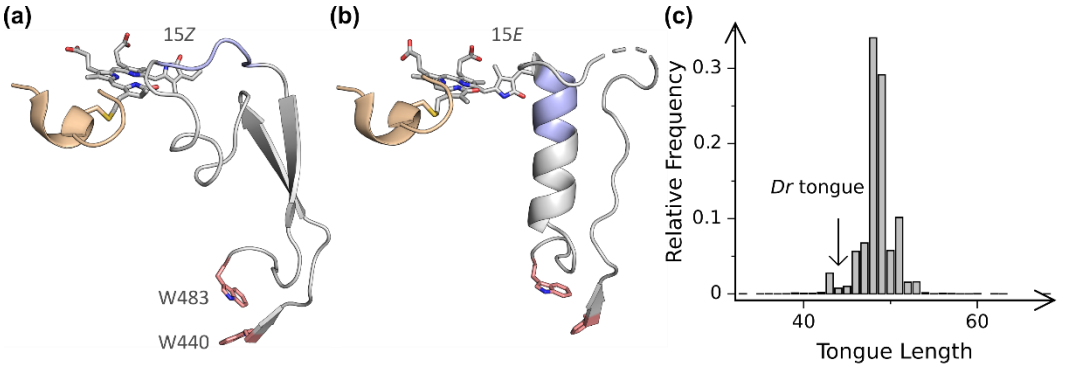

(d)

*Dr*_Q9RZA4	432	EGWSECLVWLRPELRLEVAWGG--ATPDQAKDD------LGPRHSFDTYLEEKRGYAEPWHPGEIEEAQDLRDTLTGALGERLSVIR	510
*Dd*_C1D3W9	430	GHWEEYLLWFRPEIPQTVTWGGNPAKPVQSGED--GTVDLTPRASFEAYVQQVRHTALPWHPGEVAEAESMRDALVETTSVRLTALQ	514
*As*_WP_010479127	451	PAQNIHLLWFKPEVVQTVNWGGEPKQQQGVDAE--GLPYLTPRQSFERWQETVRRKSLPWSDLAKEAVLELRGAIIGIVLKKVDELA	535
*Cc*_H8MLG4	426	PSVPHFALWFRPEVARTVAWAGNPNKPVRPEP---GHARLRPRASFDVWREEMKGASTPWSAQDLEAARALKGALVGVVLRHAEELA	509
*Is*_F7RW09	428	ADLFSYLLLFRVAQNEVRTWAGKPEKLSVETSTG---TMLGPRKSFEAWQDEVSGKSQPWRTAQLYAARDIARDLLIVADSMQLNLL	511
*Ps*_KPZ04210	544	KPIDNAVMWFRAQLTSTMNWSGDPTHHVSTRPESSASHRLHPRQSFDVWEQEVTGIARPWSRADLYGAEDIRRSALESDLERQVQRE	630
*Dc*_A0A841HYA5	434	AGWDEYIVWFRPEVPLEITWGGNPNKPVQVTAD--GTAQLTPRASFAAYVETVRETALPWHPAEVEEVSALRATLVEAQGARLTLLR	518
*Dm*_E8U3T3	430	GNWDEYLLWFRPEIPATITWGGDPHKAVQVSDD--GTARLTPRASFSSYVEAVRGVAQPWQAGDLDAALDLRGALLEVQGARLAALQ	514
*Dp*_WP_157448871	433	ERWDEYLIWFRPEAAQTIRWGGDPNKPVEVSPDT-GVRRLSPRTSFETYVQTVRHTSLPWHPVEVEAAAELRHALIEANAARTRALK	518
*Pl*_WP_019503487	443	RVQKTFIIWFRPEVIQTVDWGGNPHKPLEIESD--GSIRMSPRKSFAKWQETVKGKSLPWKPCEVEAALELRSSIVSIVLRKADELT	527
*Ac*_A8HU76	422	HRPRDYLFFFRKEAVQTVEWAGNPHKHYATGLHG---DRLTPRKSFAIWKETVEHQSWPWTQADRDFAEAARNALVEIVLRHNELLA	505
Agp1_Q7CY45	417	ELHGSWLIWFRPEVIKTVRWGGDPHKTVQES------GRIHPRKSFEIWKEQLRNTSFPWSEPELAAARELRGAIIGIVLRKTEEMA	497
Agp2_A9CI81	421	QVKSDYLLFFRKEIVQNLNWAGNPEKSYETGPMG---DRLTPRKSFAIWKETVRLQAQPWSEADREIAEAARIALVEVAFHHSELMA	504
*Av*_B9JR96	420	EIPRDYLLFFRKERLQTLNWAGNPDKSYEIGPLG---DRLTPRKSFAIWKEAVTKQSDHWSENDREVAEAIRAVTVKVVLRHNELMQ	503
*Cg*_NJK50749	429	KVQKFYILWFRPEVMQTVNWGGNPNKPVEVKNN--GEVRLSPRKSFALWQELVSNQSIHWKQCEIEAAMELRSSIVGIVLKGADELA	513
*Dl*_0OV12932	424	RSRHDYVMWFRPEELQTVTWGGDPTKPVEVAPD--GSDRLTPRRSFEAWMETVRGRSRPWQAEELAAARALRRAIMSVVLRRVEELG	508
*Hs*_W8F0E4	436	RAAGDFIIWLRPEVLQTVTWAGQQQKAEVMKD---GQLHLSPRHSFAAWSESVENTAEAWKPIEVEAAEEIRLRIADIRLKLFNEIQ	519
*Js*_CUI04487	430	RIHKHYLLWFRPEVVRTVEWAGNPHAKDGAAPM----AQLSPRTSFATWRETITGTSAAWHPGEIELATEFRTALLGIALERAEQMA	512
*Pa*_Q9HWR3	418	RQESGWIFWFRHEEVHRIRWGGKPEKLLTIGPS---GPRLTPRGSFEAWEEVVRGHSTPWSETDLAIAEKLRLDLMELCLNHAAEVD	501
*Sa*_Q097N3	433	RGRNNFVLWFRPEAVQTVNWSGNPTKAVEFDQG--GP-RLHPRKSFELWKETVRGRCLPWKAYEVEAASELRRSIIDVALQRSEELL	516
*Xc*_A0A0H2XCS3	433	PQSRSALLWTRREQIQQIKWAGNPQLAKLEDIPN---SRLSPRKSFDLWQQTVRGRARRWSPLHLESARSLRVLIELMERKRFQQDF	516

Properties of the PHY tongue. **(a)** Interaction of the biliverdin (BV) chromophore with the PHY tongue in the Pr state of *D. radiodurans* BphP (PDB identifier 4q0j, [93]). The BV cofactor adopts the 15*Z* conformation, and the PHY tongue folds into a β hairpin. The conserved PRXSF motif is highlighted in blue, and two conserved aromatic residues flanking the tongue are shown in pink. **(b)** As in panel (a) but showing the Pfr state (5c5k, [57]) with BV in the 15*E* configuration and the tongue adopting α-helical conformation. **(c)** The PHY tongue was analyzed in around 13,900 PHY-containing proteins. The plot shows the frequency distribution of the tongue lengths across these proteins. *D. radiodurans* BphP is among the proteins with the shortest tongue (indicated by arrow). **(d)** Multiple sequence alignment of the PHY tongues of the 21 BphP PCMs analyzed in this study. For species abbreviations, see Fig. 1; Uniprot identifiers are listed after the underscore character. The circles above the alignment denote the secondary structure as observed in the crystal structure of PagC (PDB 6fht) [38], with α-helices in tan, β-strands in blue, and unstructured regions in white. The conserved PRXSF motif within the PHY tongue and the most C-terminal PCM residue included in the PACs are highlighted by wide open arrows and blue shading. Two aromatic residues, highlighted by thin black arrows and red shading, denote the residue positions between which the length of the PHY tongue was evaluated. For a multiple alignment of the entire PCMs, see Suppl. Fig. S1.

Figure 3

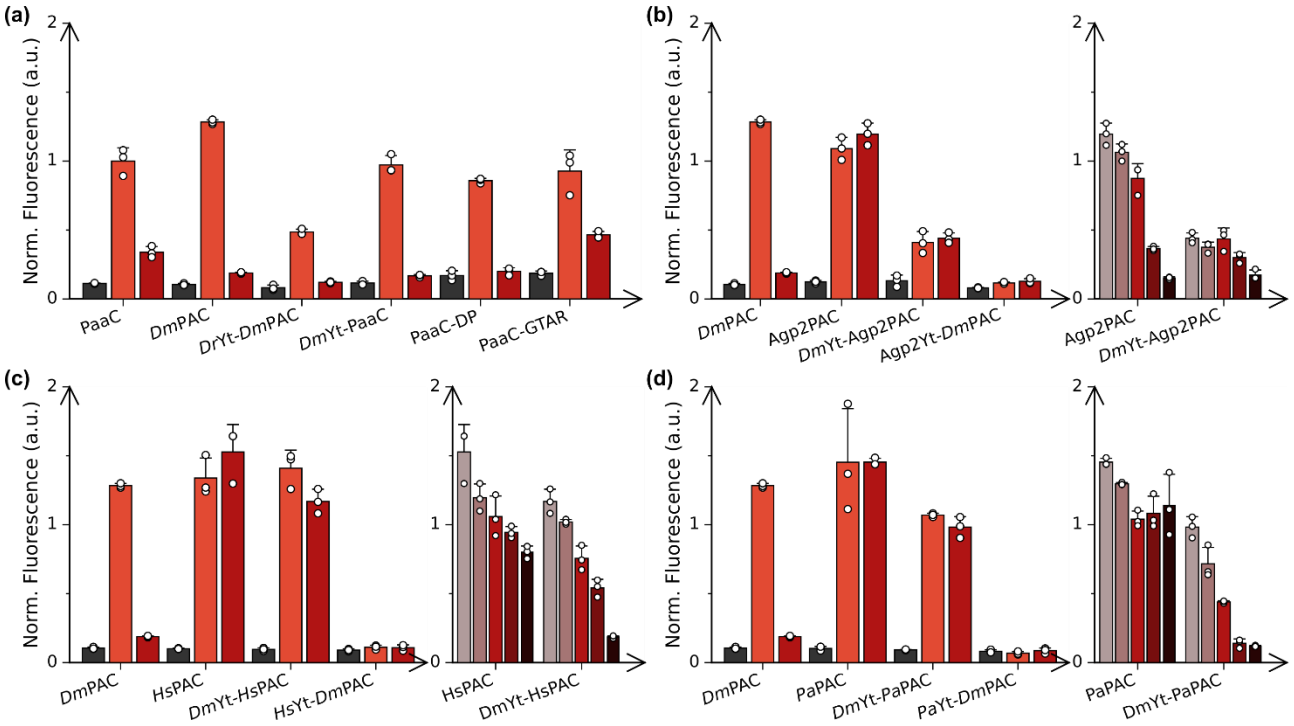

Influence of tongue exchanges on PAC activity and light repsonse. pCyclR reporter fluorescence was determined for PAC variants cultivated in darkness (black bars), under constant red light (red bars, 40 µW cm^{-2}, 660 nm), or under constant far-red light (brown bars, 240 µW cm^{-2}, 810 nm). All fluorescence values are normalized to the optical density of the underlying bacterial cultures and represent mean ± s.d. of three biologically independent samples. **(a)** *Dm*Yt-PaaC denotes the exchange of the PHY tongue for that from *Dm*PCM; *Dr*Yt-*Dm*PAC designates the converse introduction of the tongue from *Dr*PCM into *Dm*PAC. PaaC-DP and PaaC-GTAR refer to residue insertions within the PHY tongue of PaaC. **(b)** Corresponding tongue exchanges between *Dm*PAC and Agp2PAC. The right panel shows the response to illumination with 810-nm light at intensities of 240, 500, 1,000, 1,500, and 2,000 µW cm^{-2} (from left to right). **(c)** Tongue exchanges between *Dm*PAC and *Hs*PAC. **(d)** Tongue exchanges between *Dm*PAC and *Pa*PAC.

Figure 4

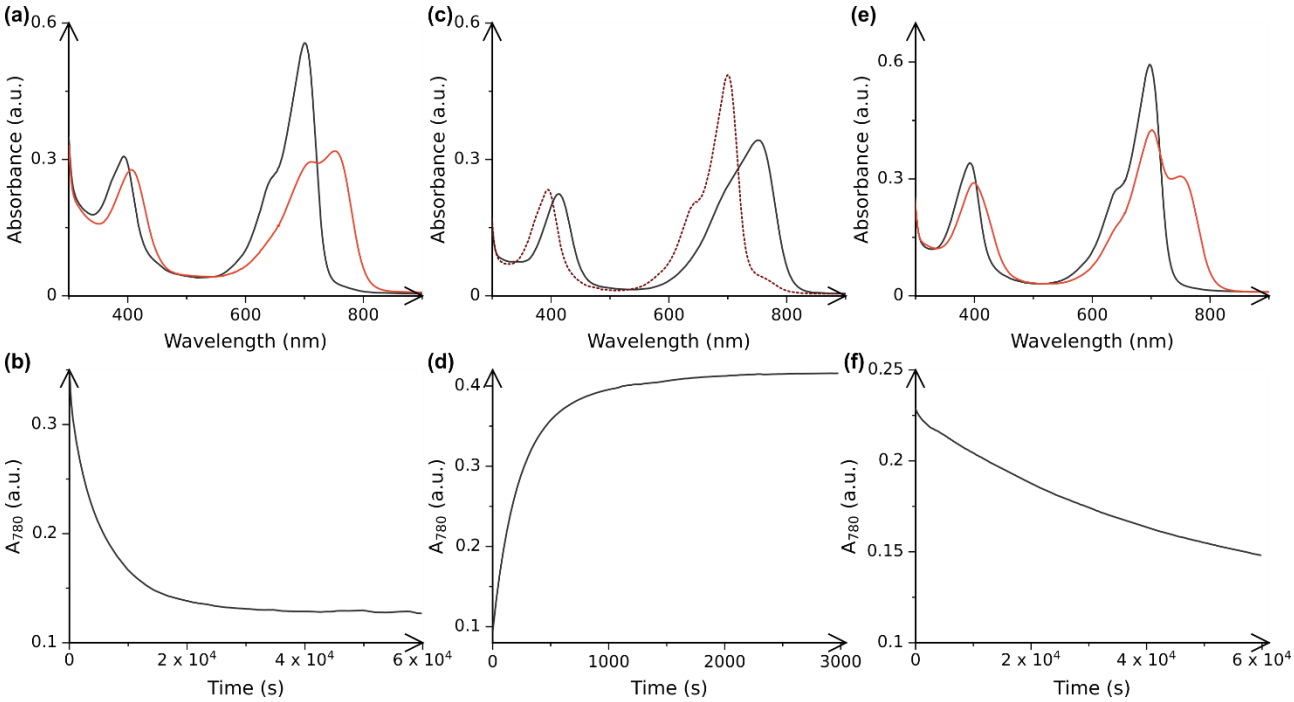

Absorbance-spectroscopic analyses of PACs. **(a)** Absorbance spectra of *Dm*PAC in its dark-adapted state (black) and after saturating illumination with 630-nm light (red). **(b)** Dark recovery of *Dm*PAC after prior red-light activation. **(c)** Absorbance spectra of *Pa*PAC in the dark-adapted state and after exposure to 780-nm light (brown, dotted). **(d)** Dark recovery of *Pa*PAC after prior far-red-light activation. **(e)** Absorbance spectra of dark-adapted *Dm*Yt-*Pa*PAC and upon illumination with 630-nm light. **(f)** Dark recovery of *Dm*Yt-*Pa*PAC after prior red-light activation.

Figure 5

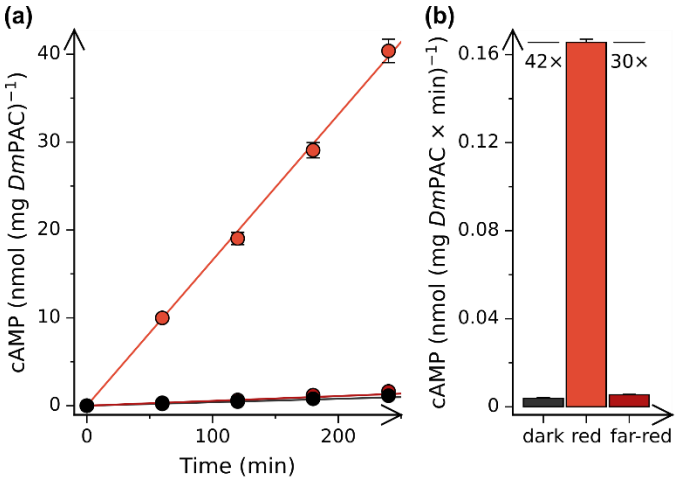

Specific enzymatic activity of *Dm*PAC. **(a)** *Dm*PAC was incubated at 30°C with an excess of substrate ATP in darkness (black symbols and lines), under constant red light (633 nm, 80 µW cm^{-2}), or under constant far-red light (810 nm, 20 mW cm^{-2}). Aliquots were taken at indicated times, inactivated by heat denaturation, and analyzed by reversed-phase high-performance liquid chromatography on a C18 column. Data points represent mean ± s.d. of three replicates. The reaction time course was fitted to a straight line to derive initial reaction velocities. **(b)** The catalytic turnover of *Dm*PAC in darkness, under red light, or under far-red light.

Figure 6

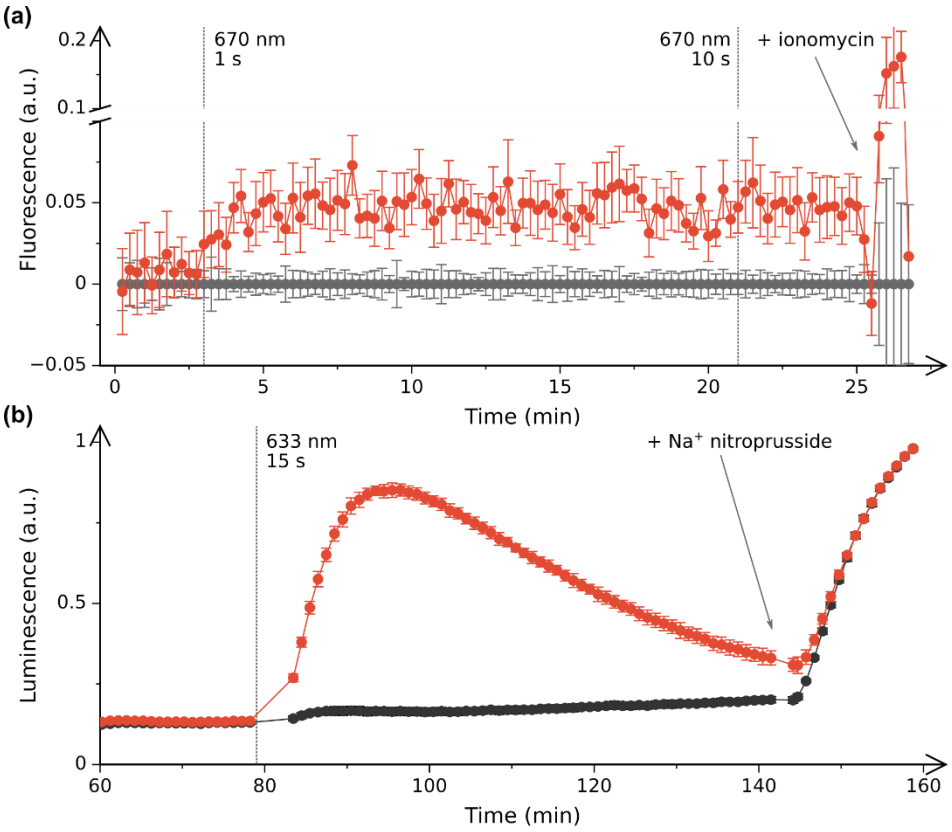

Optogenetic application of *Dm*PAC and its cGMP-specific variant *Dm*PGC in mammalian cells. **(a)** HEK-TM cells stably expressing the CNGA2-TM ion channel were transfected with a *Dm*PAC expression construct (red symbols). After loading with the Ca^{2+}-sensitive dye FluoForte-AM, the cells were incubated at 37°C, and fluorescence was monitored over time. At the indicated times (dashed lines), the cells were exposed to 40 µW cm^{-2} 670-nm light. Ionomycin was added at the end of the experiment to allow data normalization (arrow). The grey symbols denote non-transfected control cells. Data represent mean ± s.e.m. of two independent measurements with quadruplicate samples. **(b)** The cGMP-specific photoactivated cyclase *Dm*PGC was co-transfected into HEK293TN cells alongside a cGMP-sensitive luciferase. Upon incubation in darkness at 37°C, the cells were either exposed to 633-nm light for 15 s (red symbols) or left in darkness (black symbols). For normalization purposes, sodium nitroprusside was added at the end of the experiment (arrow). Data represent mean ± s.d. of 4 independent measurements.

Figure 7

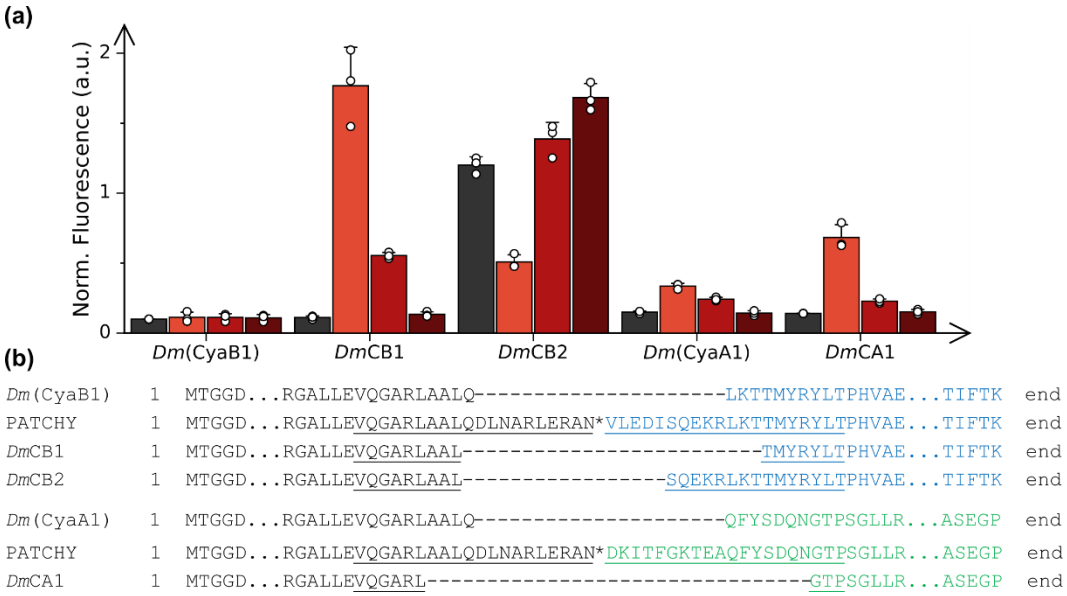

Novel PAC variants through exchanges of the cyclase effector module. **(a)** Variant PACs were generated by coupling the *Dm*PCM to the cyclase entities from *Nostoc* sp. PCC 7120 CyaB1 and *Synechocystis* sp. PCC 6803 CyaA1. Using PATCHY [63], linker modifications of these PACs were generated and screened for light-regulated activity. Representative variants exhibiting light reponses are shown and denoted as *Dm*CB1, *Dm*CB2, and *Dm*CA1. The activity and response to light of the PACs were tested within the pCyclR setup in bacterial cultures incubated in darkness (black bars), red light (red bars, 660 nm, 40 µW cm^{-2}), or under far-red light (810 nm) at intensities of 240 µW cm^{-2} (brown) and 2 mW cm^{-2} (dark brown). Fluorescence readings are normalized to the optical density of the bacterial cultures and are reported as mean ± s.d. of three biologically independent samples. **(b)** Composition of the PAC variants from panel (a). The sequence of the *Dm*PCM is shown in black, and those of CyaB1 and CyaA1 in blue and green, respectively. Based on the parental construct, the PATCHY start construct was generated by extending the linkers of the PCM and cyclase by ten residues each. In between the linkers, a frameshift, denoted by an asterisk, was inserted. Within the PATCHY scheme, the linkers could be extended or shortened on each side by 10 residues (underlined) relative to the start construct. The sequences of the PAC variants from panel (a) are indicated as well.